Mechanisms of inorganic salts on $Ca(OH)_2$-activated ground granulated blast-furnace slag curing under different temperatures

Qi Zhai [a], Kiyofumi Kurumisawa [b, *]

[a] Division of Sustainable Resources Engineering, Graduate School of Engineering, Hokkaido University, Japan

[b] Division of Sustainable Resources Engineering, Faculty of Engineering, Hokkaido University, Japan

*Corresponding author

Abstract[1]

This study investigated in detail the coupling effects of curing temperatures (5, 20, and 35°C) and additional activators (Na_2SO_4, $Ca(NO_2)_2$, NaCl, and $Na_2S_2O_3$) on $Ca(OH)_2$-activated granulated blast-furnace slag (GGBFS). The results show that the early strengths, hydration degree and microstructure of samples depend strongly on the curing temperature and the nature of activators. Activators influence considerably the initial pore solution composition and pH value, while low-pH values and high-Ca^{2+} activity suppress the dissolution of $Ca(OH)_2$ and the reaction of GGBFS. Elevated temperatures mainly accelerate the hydration of GFBFS in all samples at early age. However, owing to the cross-over effect, there is a negative effect on the properties of the samples with added sodium salts in the middle and late stages of hydration. For samples in which $Ca(NO_2)_2$ was added, the early hydration is low owing to the common ion effect, and high temperature plays a facilitating role instead. Furthermore, the apparent activation energy of GGBFS hydration was also determined to explain the observation. Results show that the sample in which the additional activator was added was influenced considerably by the curing temperature, while samples in which $Ca(NO_2)_2$ was added were more sensitive to curing temperature changes.

Keywords: Granulated blast furnace slag, Activation energy, Hydration, Activator, Kinetics

[1] **Abbreviations**

LOI	Loss on ignition
E_a	Apparent activation energy
GGBFS	Granulated blast furnace slag
AAS:	Alkali activated slag
Con:	Control
LEIC:	Limiting the equivalent ionic conductance

1. Introduction

In Japan, the annual cement production from 2010 to 2019 was approximately 59 million metric tons. This large cement production is bound to cause harm to the environment [1]. To reduce the environmental pollution caused by cement production, an extensively used method involves the replacement of part of the cement with supplementary cementitious materials (SCMs) [2–5].

Granulated blast furnace slag (GGBFS) is a latent hydraulic supplementary cementitious material which is extensively used worldwide [6]. This material is typically used as a partial replacement of Portland cement. Researchers have found that GGBFS-blended cement has good mechanical properties and chemical resistance [7]. It can also be used without Portland cement, normally in alkali activated systems [8–11]. In this situation, activators play an important role in the hydration process of GGBFS [12–15]. Gebregziabiher et al. [16] investigated the effect of sodium hydroxide (NaOH) on slag hydration at ambient and high temperatures. NaOH could produce a more rapid product than sodium silicate-activated systems at ambient temperature to improve the early strength. Cihangir et al. [17] reported the effects of water glass solution, NaOH, and sodium carbonate (Na_2CO_3) on slag hydration, claiming that the accelerator anions play a decisive role in the strength development of slag. Kondo et al. [18] reached the same conclusion through a diffusion experiment and discussed the relationship between limit equivalent ionic conductivity (indicative of the ionic mobility in solution) and the accelerating effect of different anions; the greater the acceleration of the hydration is, the higher is the anionic mobility.

Simultaneously, thermodynamic modeling has been used to study the phase assemblage and chemical composition of alkali-activated slag to investigate the process of slag hydration [10, 19–22]. Lothenbach et al. [22] used thermodynamic modeling to study different alkali-activated slag systems; alkali activators mainly influence the Ca/Si ratio of the C-(A)-S-H and the composition of pore solution. Zuo et al. [21] claimed that although the Na_2O content did not influence the type of reaction products significantly, increased Na_2O content accelerated the reaction degree of slag activated by the NaOH system. For alkali activated slag (AAS), the pH value in the pore solution plays an important role in the activation process. Usually, a high-pH value (>13.0) is required to accelerate the dissolution of slag [23]. Currently, the most common activators used in AAS are NaOH and sodium silicate, which lead to problems, such as toxicity and high costs [24, 25]. $Ca(OH)_2$—a more practical and less expensive activator—has been demonstrated to have activating efficacy by many researchers [14, 26, 27]. Regarding the $Ca(OH)_2$ activated slag system, the pH of the pore solution is approximately 12.5 at ambient curing temperatures. Therefore, additional activators are always added to accelerate the initial dissolution and hydration of slag to obtain better mechanical properties at an early age [28–30]. Jeong et al. [14] showed the influence of four additive activators on the $Ca(OH)_2$-activated slag system, and reported that the additive activator could improve the early strength, although the late strength could not be improved. Yang et al. [29] studied the effects of $Ba(OH)_2$ as an additional activator of the $Ca(OH)_2$-activated slag system, and concluded that the addition of 1% $Ba(OH)_2$ can improve the stabilization of C-(A)-S-H gels in the long term. However, few researchers have investigated the phase transformations and the corresponding volumetric change of $Ca(OH)_2$-

activated slag under the coupling effect of temperature and activators.

From the perspective of kinetics, Ben Haha et al. [31] concluded through experiments that the type of alkaline activator has a greater impact on the hydration kinetics, strength development, and hydration products of slag than the chemical composition of slag itself. Biernacki et al. [30] investigated the reaction constants and activation energies of various slag/$Ca(OH)_2$ ratios at different temperatures, and concluded that the hydration of slag in cement agrees well with the activation energy of slag in the presence of $Ca(OH)_2$ alone. The hydration mechanism of slag is quite different from those of cement and cement slag binders; in particular, the hydration of slag is easily affected by the pH value [32–35]. Li et al. [35] investigated the effects of temperature and pH on the early hydration rate of alkali-activated slag, and reported that the activation energy of slag increases as a function of pH. Additionally, increasing the temperature in a low-pH environment can promote hydration. Many researchers have shown that the effect of temperature on slag hydration is also important [36–41]. Yang et al. [40] observed the strength and microstructure development of alkali-activated slag in low-temperature curing conditions, and reported that although slag can be hydrated at low temperatures, the hydration degree and strength are low, and the porosity and macroporosity are increased. Wei et al. [42] also concluded that low-temperature curing results in the formation of harmful pores. Shumuye et al. [38] found that high-temperature curing can reduce the early drying shrinkage of alkali-activated slag concrete and improve the early strength, but the later strength is reduced owing to the distribution of heterogeneous hydration products. Aziz et al. [43] found that the apparent porosity of GGBFS-blended cement in high-temperature curing conditions was higher than that under low-temperature curing. However, few researchers have investigated the effects of different curing temperatures on $Ca(OH)_2$-activated slag.

In a previous study, we investigated the effects of activators, such as sodium sulfate (Na_2SO_4) and calcium nitrate ($Ca(NO_2)_2$) on $Ca(OH)_2$-activated GGBFS at low temperatures [44]. At low temperatures, the hydration degree of GGBFS slows down, and the pore structure of the GGBFS after hydration cannot be effectively improved, which restricts the development of compressive strength. Specifically, the added $Ca(NO_2)_2$ increases the calcium concentration in the system, which contains abundant soluble $Ca(OH)_2$ quantities, and results in a pH reduction owing to the suppression of $Ca(OH)_2$ by the common ion effect of calcium. However, the effect of activators on GGBFS hydration in high-temperature curing conditions has not been investigated. The additional activators used in this study were Na_2SO_4, $Ca(NO_2)_2$, and NaCl, which are based on previous studies [44, 45]. In addition, recently, some studies have demonstrated that the effect of sodium sulfate in improving the cement hydration process is stronger than that of sodium thiosulfate ($Na_2S_2O_3$) at the same content [46, 47]. The effect on GGBFS hydration has not been investigated. Therefore, $Na_2S_2O_3$ is also investigated in this study to form a control group with Na_2SO_4 subject to the condition that the content of Na_2O is maintained the same. The main aim of this study was to investigate the influence mechanism of inorganic activators on $Ca(OH)_2$-activated GGBFS at different temperatures, the influence of inorganic salts on the reaction rate of GGBFS, the phase transformation of GGBFS hydration products, microstructural changes at different temperatures, and changes in porosity through a thermodynamic model.

2. Experimental

2.1.Materials and mix proportion

GGBFS (density:2.91 g/cm^3, specific surface area:3850 cm^2/g) and calcium hydroxide (density: 2.24 g/cm^3) used were the same as those used in previous research studies [44]. The chemical compositions and physical properties are listed in Table 1. The particle size distribution of raw materials is shown in Fig. 1. Fig. 2 shows the X-ray diffraction analysis of GGBFS, which suggests that the GGBFS is mainly composed of an amorphous phase. The activators were prepared by dissolving analytical-grade Na_2SO_4, $Ca(NO_2)_2$, NaCl, and $Na_2S_2O_3$ inorganic salts, which show remarkable promotion effects at the appropriate doses [44, 45, 48, 49] (in deionized water at a dose of 0.1 mol/kg). Table 2 lists the compositions of the pastes. For mortar, the binder/sand ratio was 1:3. The others were the same as the paste. To mix the mortar, the dry GGBFS, $Ca(OH)_2$ powder, and sand were first poured into the bowl for low-speed mixing for 30 s; the pre-prepared solution was then poured for low-speed mixing for 90 s; this was then paused for 30 s. During this period, a trowel was used to scrape down the binders on the edge and mixing blades to maintain homogeneity. Finally, the mixture was mixed at a high speed for 2 min. The process of mixing the paste was the same as that for the mixing of mortar, except that no sand was used. The mortar was cast into a cylinder (diameter: 50 mm, length: 100 mm), and the paste was cast into a plastic cylinder (50-mm diameter and 50-mm length). The samples were sealed with a plastic film to minimize the carbonation and moisture exchange with air. Subsequently, the samples were placed in standard curing chambers at 5, 20, and 35°C until the measuring ages of 3, 7, and 28 days. The mortar samples were used for the mechanical tests, and the pastes were used for microstructural analysis. At the corresponding curing age, the solvent exchange method was used to stop hydration of samples. The pastes were crushed into smaller specimens using a hammer, and then immersed in acetone for 2 h. The specimens were then surrounded by a carbon dioxide absorbent (YABASHI Lime-*f*) and stored in a curing chamber at a constant temperature of 40°C for 1 day to dry. Before testing, all the specimens were stored in vacuum bags. For X-ray diffraction (XRD), selective dissolution, and NMR tests, the specimens were ground into powder using a ball mill. The powder was prepared by grinding in a planetary ball mill at 200 revolutions per minute (rpm) for 6 min. The powder was milled further in an agate mortar and the particle size was less than 300 μm.

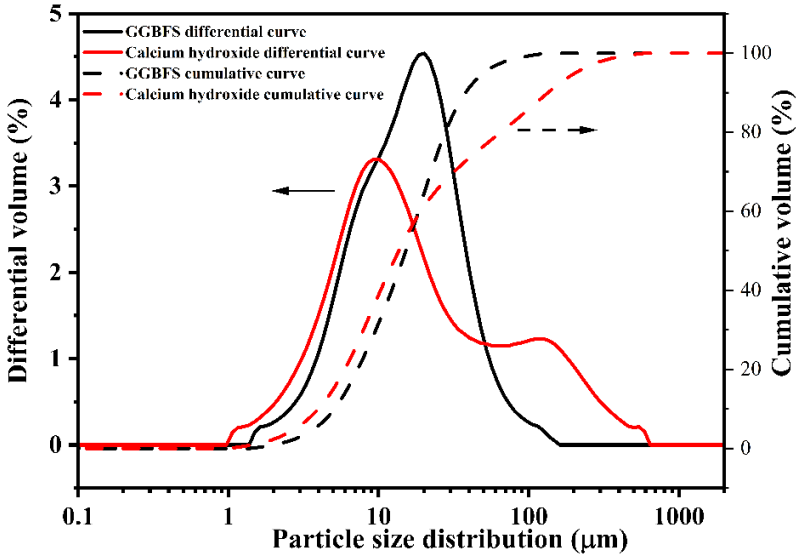

Fig. 1. Particle size distribution of granulated blast furnace slag (GGBFS) and calcium hydroxide.

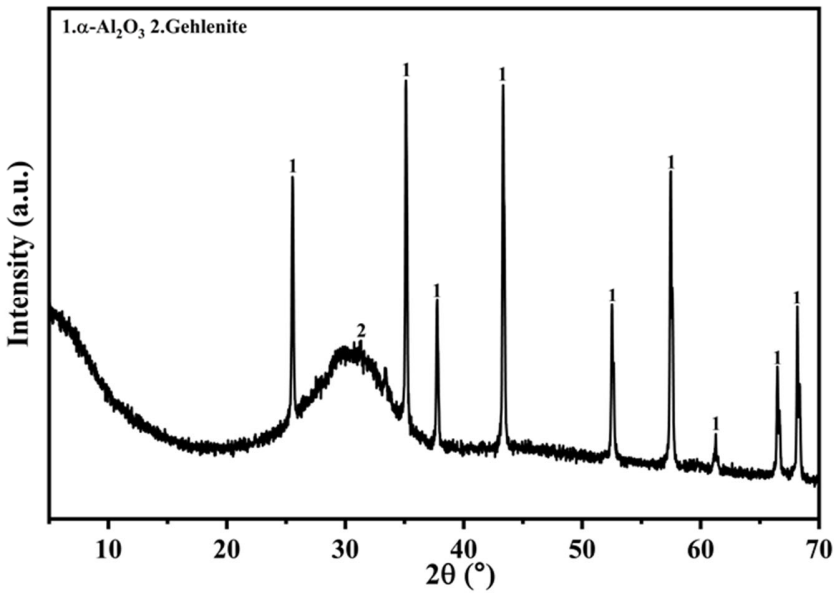

Fig. 2. XRD analysis of GGBFS

Table 1

Chemical composition of granulated blast furnace slag (GGBFS) and calcium hydroxide

	Chemical composition (mass%)										
GGBFS	CaO	SiO_2	Al_2O_3	MgO	SO_3	Fe_2O_3	TiO_2	Na_2O	K_2O	MnO	Others
	41.8	33.8	13.3	7.2	0.7	0.7	0.5	0.4	0.3	0.2	0.1
Calcium hydroxide	$Ca(OH)_2$	$CaCO_3$	Others								
	97.5	1.0	1.5								

Table 2

Mix proportions of pastes

Identity (ID)	GGBFS g (wt%)	$Ca(OH)_2$ (wt%)	Water/$Ca(OH)_2$ - GGBFS binder ratio	Curing temperature	Accelerator (wt% of binder)
Con	80	20	0.55	"5°C" "20°C" "35°C"	/
Na_2SO_4					1.42%
$Ca(NO_2)_2$					1.5%
NaCl					0.585%
$Na_2S_2O_3$					1.58%

Abbreviations for notation: Con, control group.

2.2.Testing methods

2.2.1. Compressive strength

The compressive strength was measured at 3, 7, and 28 days in samples demolded on the same day using an automatic testing machine (Hi-ACTIS-2000). The average value of the three mortars was reported as the compressive strength.

2.2.2. X-ray diffraction

Powder X-ray diffraction (XRD, MultiFlex Rigaku Co., Ltd., Tokyo, Japan) was used to investigate the crystal phases. The measurements were conducted using Cu-Kα radiation at 40 kV and 40 mA. We added 20% α-Al_2O_3 in the samples, which was used as an internal standard. All the samples were scanned in the range of 5–70° (2θ)at 0.02° steps, and with a scan speed of 2°/min.

2.2.3. Solid state nuclear magnetic resonance (NMR)

^{29}Si DD MAS-NMR spectra (119.26 MHz) and ^{27}Al MAS-NMR (156.41 MHz) spectra were collected on a solid-state NMR spectrometer (AVANCE III600WB) to study the polymerization of the hydration products. The spinning rate was 12 kHz, and the repetition delays were 20 and 5 s, respectively.

2.2.4. Isothermal calorimetry

Isothermal calorimetric tests were conducted using a MMC-5116 (Tokyo Riko)

instrument set at 5, 20, and 35°C. Approximately 20 g of binder was mixed outside the machine for 5 min in a 100 mL ampoule. The samples were then placed in a calorimeter. Because of the temperature difference inside and outside the chamber, measurements during the initial hour were omitted [50].

2.2.5. Loss on ignition (LOI)

Around 1.0 g specimen was dried in a 105°C constant chamber for 1 day to determine the moisture content. The dried specimen was then heated in air at 700°C for 2 h to obtain the LOI, as above 700°C, S^{2-} will be oxidized to sulfate to increase the mass [51]. The calculation formula is as follows,

$$LOI = \frac{m_{105°C} - m_{700°C}}{m_{700°C}} \quad (1)$$

where $m_{105°C}$ is the mass of the specimen at 105°C, and $m_{700°C}$ is the mass of the specimen at 700°C.

2.2.6. Selective dissolution

The reaction degree of GGBFS was determined by the selective dissolution. The technique adheres to that proposed by Villagrán–Zaccardi [52]. In brief, 250 mL of triethanolamine and 93 g of ethylenediaminetetraacetic acid (EDTA) were dissolved in 500 mL distilled water, and 173 mL diethylamine was added and diluted to 1 L. The powder and filter papers (diameter: 4.5 μm) were dried in an oven at 105°C oven for 1 h before the test. Subsequently, 0.5 ± 0.02 g powder was mixed with 50 mL of the solution in a beaker and then diluted to 800 mL. The solution was stirred continuously at 300 ppm for 2 h. The residue was dried in an oven for 1 h. Finally, the weight of each residue was calculated. Before the test, the dissolution of raw GGBFS was conducted to determine the undissolved proportion of the material; approximately 94.5 ± 1 wt% remained, which was within an acceptable range [52]. This result was used to correct some errors caused by the dissolution of GGBFS. Because the hydrotalcite-like phase generated during the hydration period could not be dissolved by EDTA solution, assuming that all the MgO was converted into a hydrotalcite-like phase, the mass of this phase was calculated at a mass ratio of 1:2.35 [53]. The reaction degree (α) of the GGBFS was calculated using Lumley's formula [54],

$$\alpha = \frac{100fR_p - R_b}{100fR_p - 2.35fM_{MgO}} \quad (2)$$

where *f* is the mass fraction of raw GGBFS in the dry binder, R_p is the mass fraction of GGBFS undissolved in EDTA solution, R_b is the mass fraction of the paste' s residue in g/100 g anhydrous binder, and M_{MgO} is the MgO content in GGBFS.

Dried paste (100 g) was then converted to anhydrous binder using the following formula [52],

$$m_{anhydrous} = \frac{m_{dried\ paste}}{1 - LOI} \quad (3)$$

2.2.7. Mercury intrusion porosimetry (MIP)

The pore-size distribution and porosity of pastes was analyzed by MIP. Approximately

1 g of the crushed paste specimen was used for MIP (Micromeritics Auto Pore V 9600). The pressure was up to 61,000 psia to measure the porosity, and the contact angle was 130°.

2.2.8. pH of pore solution

Before the specific age (1, 3, 6, 9, 12, 15, and 18 h), the samples were stirred every 30 min to avoid the influence of bleeding on the experimental results. The pore solution cured at a specific age was extracted by centrifugation (KUBOTA 3700) at 4000 rpm for 60 s. The obtained solutions were used for pH and concentration analysis.

2.2.9. Composition of pore solution

The collected solutions were filtered with a 5 mL medical injection device and stored at 5°C before testing. To investigate the influence of temperature and inorganic salts on the early stages of hydration, the filtered pore solutions at 1, 3, 6, 9, 12, 15, and 18 h were diluted 50-fold in the controls (Con) and 500-fold in the other samples with 2% HNO_3. ICS-90 ion chromatography (DIONEX, Sunnyvale, CA, USA) was used to determine the concentrations of Na^+ and Ca^{2+} in a cica-reagent cation mixed standard solution (07197-96, Kanto Chemical Co. Inc.).

2.2.10. Thermodynamic modeling

Thermodynamic modeling was performed using the Gibbs free energy minimization software GEMS with the CEMDATA 18 database and the CNASH_ss model [10]. The effects of inorganic salts on the phase transformation of the GGBFS were simulated in this program based on the hydration degree calculated by selective dissolution.

3. Results and discussion

3.1.Compressive strength

The results of the compressive strengths at 3, 7, and 28 days are presented in Fig. 3. The results indicated that the early age strength was promoted considerably following curing temperature increases. Compared with Con, almost all activators can increase the compressive strength at 3 days, irrespective of the curing temperature. At 7 days, except for the samples cured at 35°C, the strength cured at 5 and 20°C increased to some extent compared with that of Con. At 35°C, except for $Ca(NO_2)_2$, the strengths of all the samples with added activators were almost the same and lower than that of Con. At 28 days, except for the samples cured at 5°C, the strength of Con surpassed those of all other samples at the corresponding temperature. In particular, for the samples cured at 35°C, the strength of the same sample cured at 35°C was the highest before the age of 28 days, but at the age of 28 days, the strength of the same sample cured at 35°C was considerably lower than that of the sample cured at 20°C, which is similar to the results reported by other researchers [33, 43, 55, 56]. Many researchers call this phenomenon the crossover effect [57–59]. High temperatures promoted the decomposition of GGBFS, and resulted in the formation of more rapid products, especially the formation of C-(A)-S-H products, which filled the pores and enhanced the early strength. However, the thick shell of this gel seriously hindered the dissolution of the GGBFS, and led to the slow development of strength in the later stage.

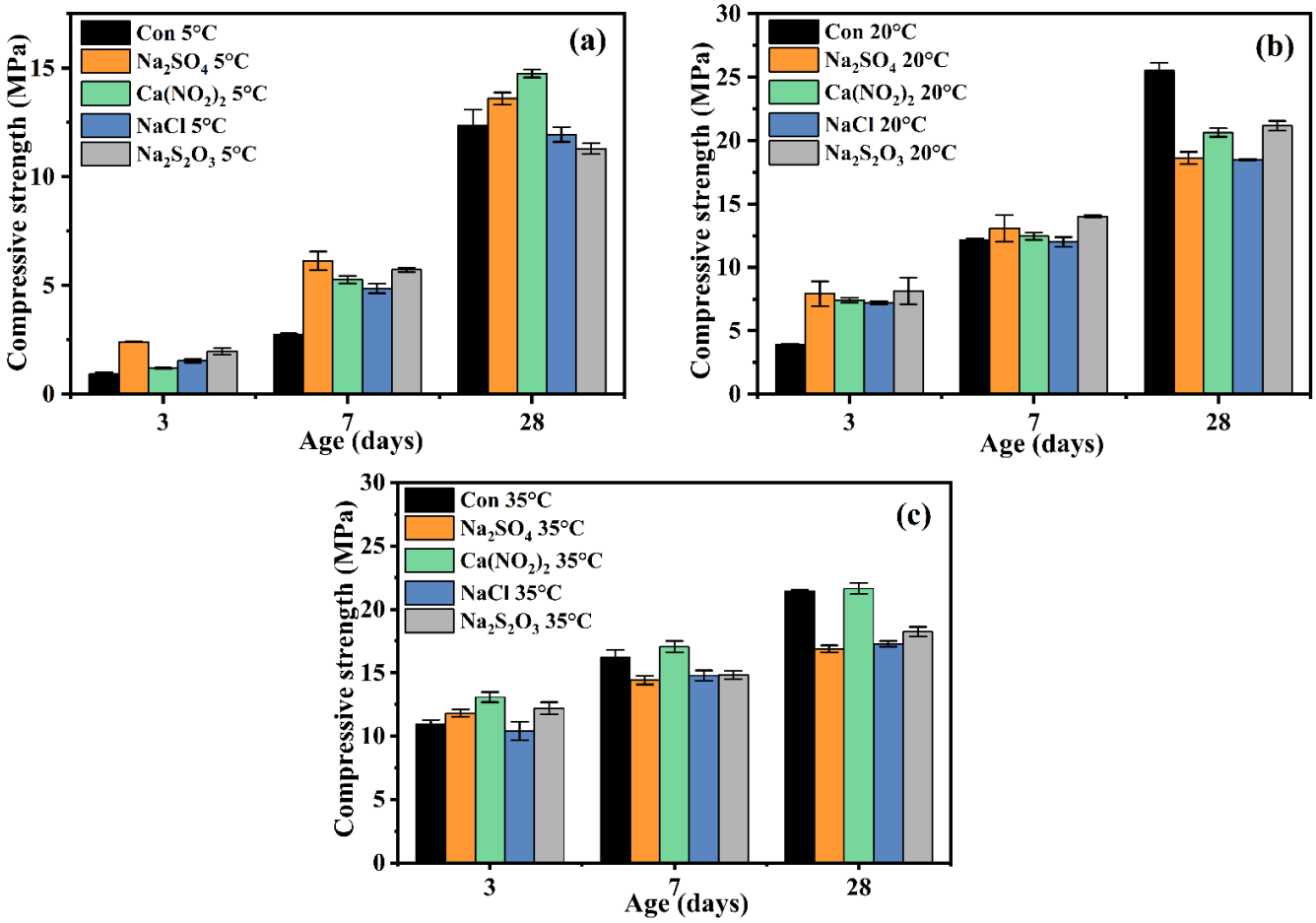

Fig. 3. Compressive strength of mortars at 3, 7, and 28 days. Curing at (a) 5°C, (b) 20°C, and (c) 35°C (Con: control).

Overall, the activators used in this study can effectively promote the early strength of GGBFS, especially at 20°C. $Ca(NO_2)_2$ showed excellent performance in strength development in the middle and late stages. The effect of NaCl on the compressive strength was the smallest compared with that of the other three activators, irrespective of the curing temperature and age. Na_2SO_4 and $Na_2S_2O_3$ showed evident and similar promoting effects on compressive strength in the early stage, irrespective of the curing temperature. This proves that the anion of the activator plays a decisive role in the strength development of GGBFS, which will be further discussed in Section 4.2. Activators undoubtedly promoted the decomposition of GGBFS at an early stage, but the hydration products differed according to the different anions of the activators. This affected the development of strength to a certain extent. The next section will discuss further the hydrates transformation by XRD.

3.2.X-ray diffraction

The XRD patterns of the pastes at a curing age of 3 days are shown in Fig. 4. Evidently,

the temperature only changed the amount of hydration products but did not change the category of hydration products. Consistent with previous studies [14, 17], the results showed that C-A-S-H, calcium monosulfoaluminate (AFm), and hydrotalcite were the main hydration products in all $Ca(OH)_2$-activated GGBFS pastes. The AFm-type phases were determined by the accelerator type. In the Con group, OH-AFm was observed at 11.30° [60]. NO_2-AFm was detected at 11.08° in $Ca(NO_2)_2$ [61, 62]. Friedel's salts at approximately 10.94° [61–64] were observed in NaCl, and the formation was always intensive, irrespective of the curing temperature. In Na_2SO_4, SO_4-AFm and ettringite (AFt) were detected at an early age. In $Na_2S_2O_3$, both AFt and the U-phase ($4CaO{\cdot}0.9Al_2O_3{\cdot}1.1SO_3{\cdot}0.5Na_2O{\cdot}16H_2O$), a phase containing Na ions, were observed at approximately 8.5° [65, 66] at three different curing temperatures [67]. Li et al. [68] argued that the U-phase can only be formed in highly alkaline conditions in the presence of sulfate and alumina. In this study, GGBFS was the only source of alumina, which showed that $Na_2S_2O_3$ promoted considerably the dissolution of GGBFS, even in a low-temperature curing environment. In addition, a considerable amount of U-phase transferred to ettringite in this study, even at the age of 28 days (see Fig. S1), this may be related to the reversible conversion process between U-phase and AFt, which will be further discussed in section 4.3.

The results of the XRD patterns suggest that activators can effectively promote the dissolution of GGBFS at an early age. Compared with Con, the main hydration products produced in large quantities provide support for strength, which is consistent with the compressive strength results.

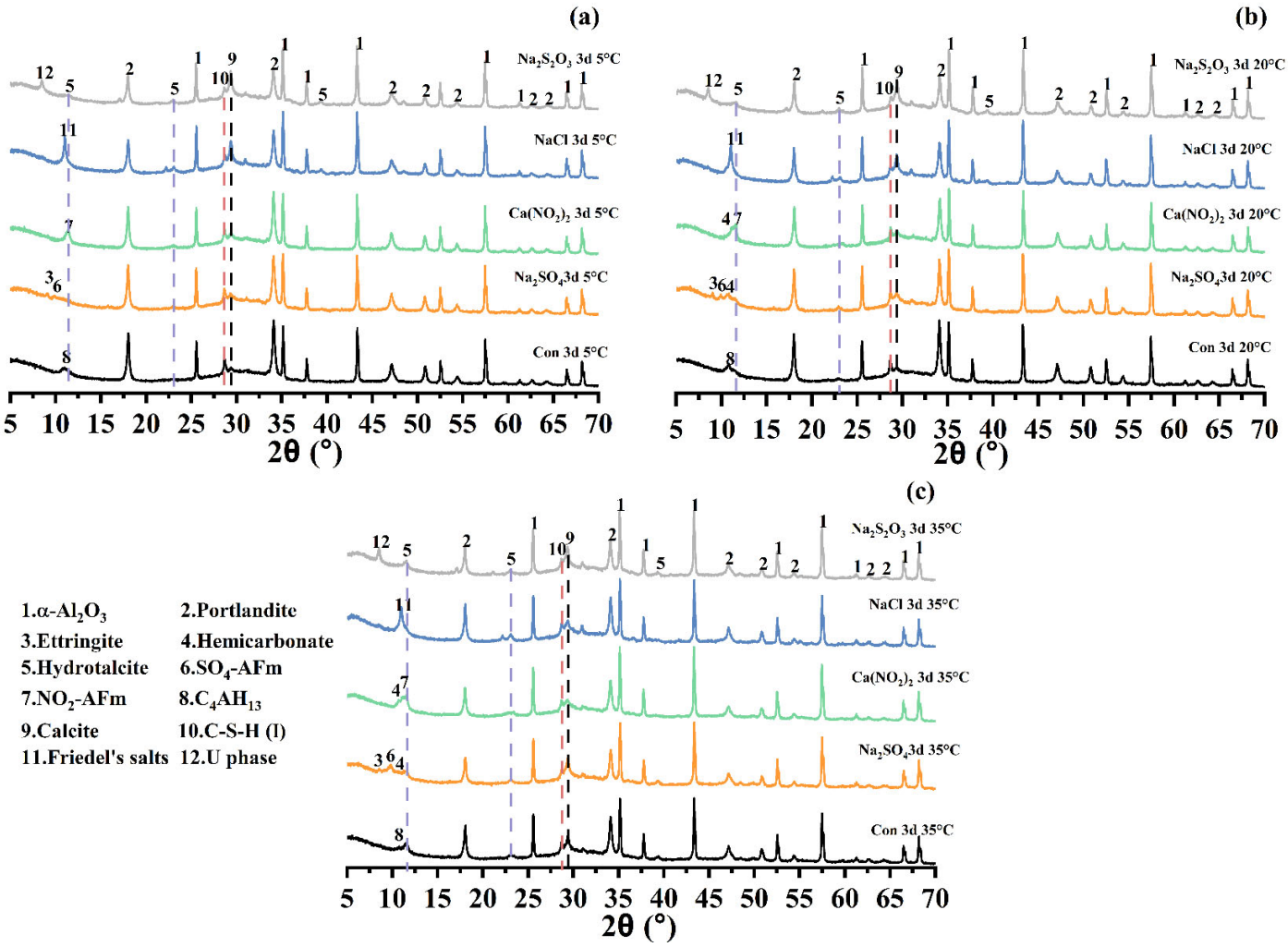

302 Fig. 4. XRD patterns of pastes cured for 3 days, Curing at (a) 5°C, (b) 20°C, and (c) 35°C.

303

304 *3.3.Solid state NMR*

305 Because GGBFS was the only source of Si and Al in this study, all curves were normalized
306 by dividing the integrated area of the GGBFS curve. In a previous study, with the exception
307 of NaCl and $Na_2S_2O_3$, the results of the other samples cured at 5 and 20°C were investigated
308 (S2). This section mainly focuses on the samples cured at 35°C at the initial stage. The
309 experimental results at 3 days of the NMR spectra are shown in Fig. 5. The ^{27}Al NMR spectra
310 ranging from -20 to 100 parts per million (ppm) of raw GGBFS and samples cured for 3 days
311 at 35°C are shown in Fig. 5a. A broad peak ranging from 20 to 90 ppm, centered at
312 approximately 64 ppm, was observed in the raw GGBFS spectrum. Two obvious peaks at
313 approximately 9.5—regarded as AFm or hydrotalcite [69] —and at 4.7 ppm—regarded as

amorphous or third aluminate hydrate [70]—were observed in the spectra of all samples. These peaks were also observed in the spectra of cement GGBFS binders [49, 71]. As shown by the spectra, the integral areas of the curves of all samples in the range of 40–80 ppm were approximately the same, and Con was slightly higher. Therefore, through the peak area of the aluminate hydrate in the range of 2–14 ppm, the hydration degree can be analyzed qualitatively even without deconvolution. Obviously, the AFm peak intensity of the samples with added activators was stronger than that of the control, which means that the activators promoted the dissolution of GGBFS. No peak related to AFt was observed around 13 ppm in the spectra of the samples cured at 35°C, even for $Na_2S_2O_3$ and Na_2SO_4 which contained more sulfur, which is quite different from the samples cured at 5 and 20°C. In a previous study [44], it was confirmed by XRD (S3) that AFt existed in the early stage of Na_2SO_4, but only SO_4-AFm remained in the later stage, thus indicating that a high-curing temperature promotes the hydration of the binder and promotes phase transformation because AFt is sensitive to higher temperatures [8, 9].

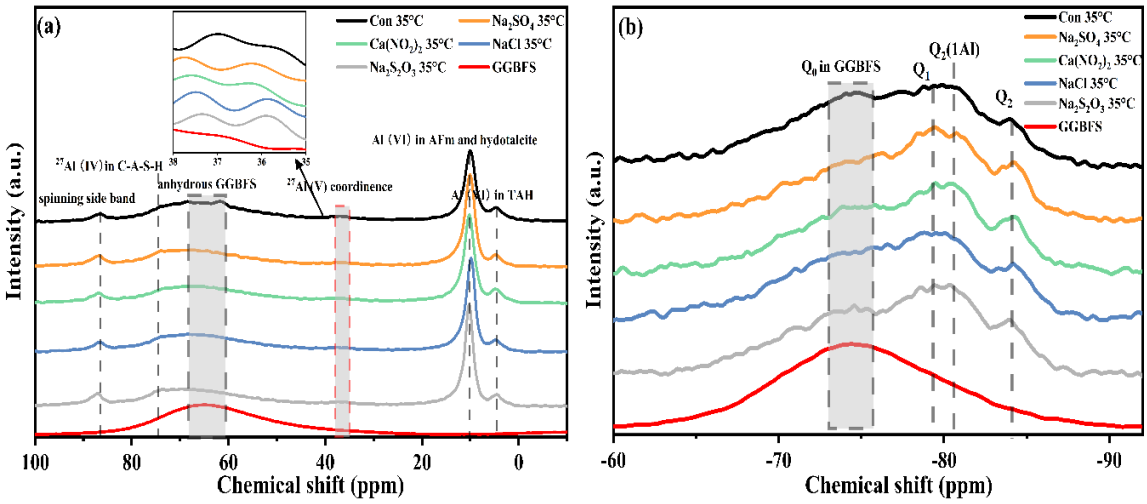

Fig. 5. NMR spectra at of samples cured for 3 days at 35°C (a) ^{27}Al MAS-NMR and (b) ^{29}Si MAS-NMR.

Fig. 5b shows the ^{29}Si NMR spectra of samples cured for 3 days at 35°C, which was used to investigate the coordination of Al in C-(A)-S-H and the substitution of Si by Al. The peaks at approximately -74, -78.9, -80.9, and -84.0, were assigned to Q^0, Q^1, Q^2(1Al), and Q^2, respectively [70, 72]. Compared with the samples cured at 5 and 20°C, the chemical shift is obvious, which means that high curing temperature effectively promotes the hydration of GGBFS at an early age. The influence of curing temperature and additional activators in the GGBFS reaction will be discussed further in the next section.

3.4.Isothermal calorimetry

Because of the temperature difference inside and outside the calorimeter chamber, the measurements of the initial hour were omitted. Fig. 6 shows the calorimetric curves of the

GGBFS pastes.

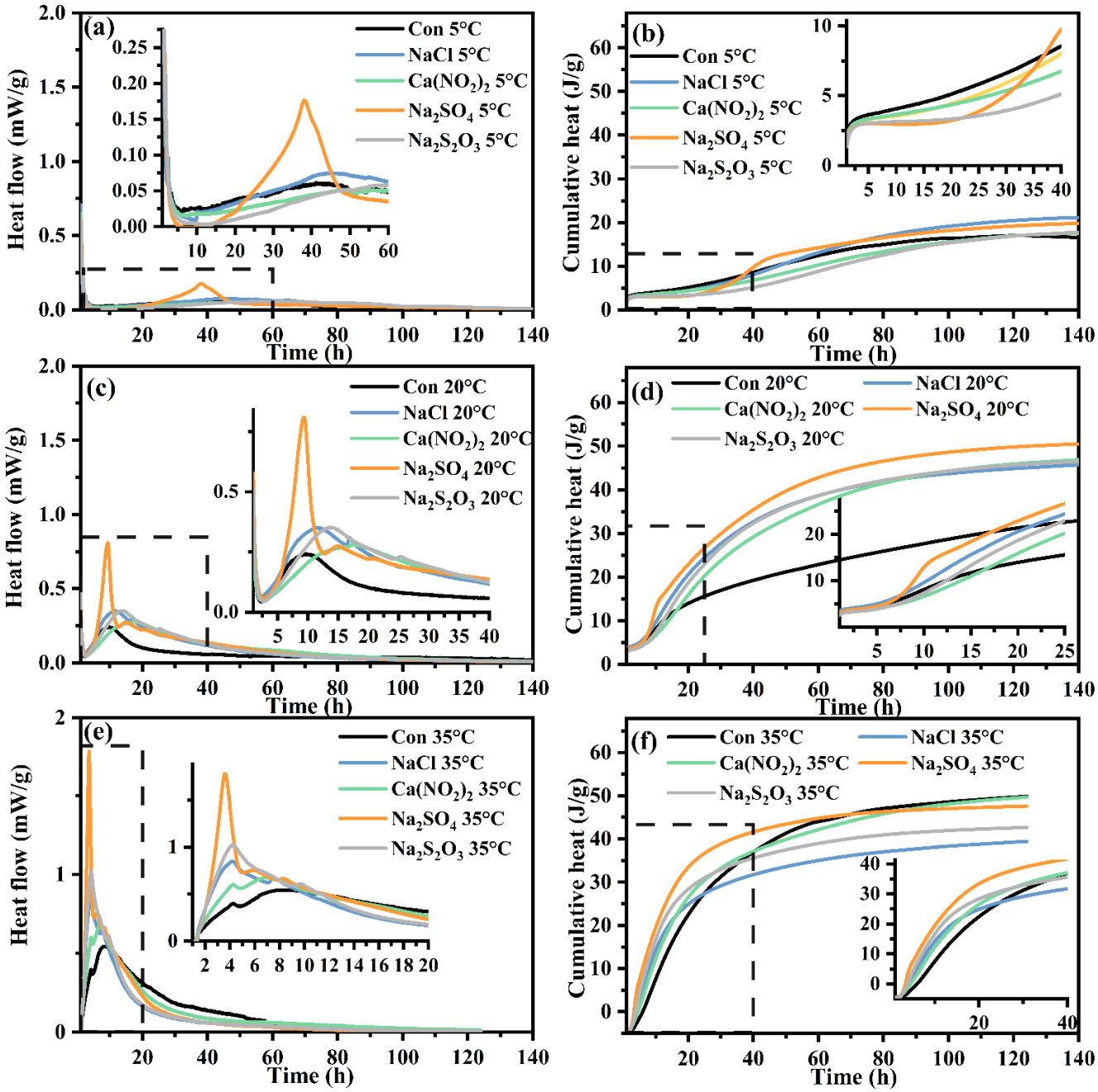

Fig. 6. Calorimetric curves of pastes: (a) heat flow at 5°C, (b) cumulative heat at 5°C; (c) heat flow at 20°C, (d) cumulative heat at 20°C, (e) heat flow at 35°C and (f) cumulative heat at 35°C.

With the exception of Na_2SO_4, at 5°C, no evident peak appeared (Fig. 6a), and the

difference between cumulative heat was small (Fig. 6b). At 20 and 35°C, the cumulative heat values of samples with added activators was higher than that of Con at an early age, especially Na_2SO_4, which yielded the highest value (Fig. 6d and Fig. 6f), consistent with the early-strength observations.

At 20°C, a wide exothermic peak appeared in the Con group at approximately 9 h; all samples with added activators yielded two exothermic peaks corresponding to the formation of hydration products after the initial 3 h. This is because Con cannot provide additional anions. Thus, the main hydration product in the early stage is OH-AFm and the peak shape of the samples, except Con, depends on the type of accelerator, which is consistent with the XRD results (see Fig. 18). With the exception for Na_2SO_4, the main peak of the other samples appeared later than that of the Con (Fig. 6c). In alkali activated GGBFS systems, activators could accelerate the dissolution of GGBFS. However, depending on the types of activators, the dissolution of $Ca(OH)_2$ may be retarded [8, 9], which will be further discussed in section 4.3.

At 35°C, the primary peak of all samples was earlier than that of samples cured at 20°C, and the samples with added activators were earlier than those of the Con samples; an obvious phenomenon is that the peak shapes of the curves of all samples changed, and the heat release was more concentrated than that at 20°C; the bulk of the heat evolution subsided within 20 h, which showed that high temperature promoted the consumption of Al in the form of AFm, and accelerated the dissolution of GGBFS; this resulted in more rapid hydration (Fig. 6e).

Fig. 7 shows the cumulative curve comparison of pastes cured at 20 °C and 35°C. At the initial stage, the cumulative heat of the pastes cured at 35°C was larger than that at 20°C. This means that the high temperature provided more energy necessary to overcome the barriers to continue hydration, and the cumulative heat flow for the different activators indicates more heat evolved and a higher hydration degree (Fig. 8). However, after 72 h, with the exception for Con and $Ca(NO_2)_2$, the situation reversed. The noteworthy point is that at 120 h, several samples completed the heat accumulation processes. According to the analysis of section 4, excess Ca^{2+} in $Ca(NO_2)_2$ leads to an increase in Ca^{2+} concentration and reduces the pH value of the pore solution, thus resulting in an impediment to the dissolution and reaction of the GGBFS at an early age. With the development of hydration, the Ca^{2+} in calcium nitrite are gradually consumed and the hydration rate of the GGBFS is enhanced, thus resulting in more cumulative heat approximately equal or even exceeding those of the other samples, especially at high-curing temperature.

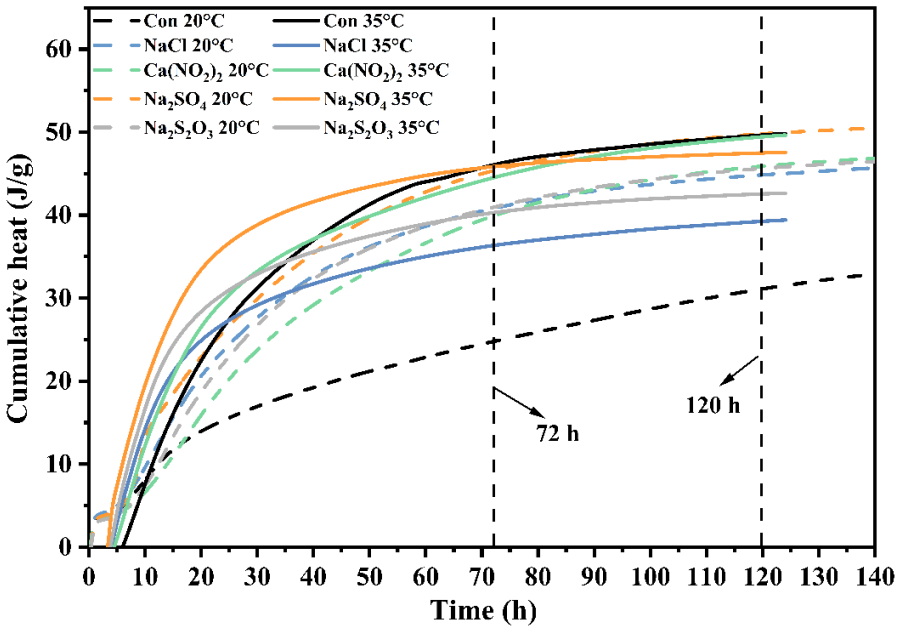

Fig. 7. Comparison of cumulative heat release of pastes cured at 20 and 35°C.

3.5.Reaction degree of GGBFS by selective dissolution

The reaction degree of GGBFS was calculated according to Eqs. (2) and (3). The results of the LOI are provided in the Supplementary Information (Table S1). Fig. 8 shows the reaction degree of the GGBFS and the relationship between the reaction degree of GGBFS and compressive strength. Regardless of the curing temperature, the hydration degree of all samples with added activators was higher than that of Con, especially at 3 days; this means that the activators effectively promoted the reaction of GGBFS at the initial stage. Evidently, with the increase in curing temperature, the reaction degree of GGBFS also increased. The GGBFS reaction degree of Con cured at 5°C was always the lowest. At 20 and 35°C, the difference between the reaction degree of the same sample cured at 20 and 35°C was very small at 7 and 28 days, which was consistent with the development of strength, as shown in Fig. 8d. However, in the later stage of hydration, the hydration degree of some samples with added activators was not very consistent with the development trend of strength, especially for the samples cured at high temperature. This shows that in addition to the hydration degree, many factors influence the development of strength in the later stage of GGBFS.

Activators can effectively promote the hydration degree of GGBFS at the initial stage, irrespective of the curing temperature, which is consistent with the development of compressive strength. Other influencing factors need to be considered when the hydration reaches a certain degree. For this reason, the next section will discuss the changes in microstructure from a microstructural point-of-view induced by the curing temperature and additional activators, and the effects on strength.

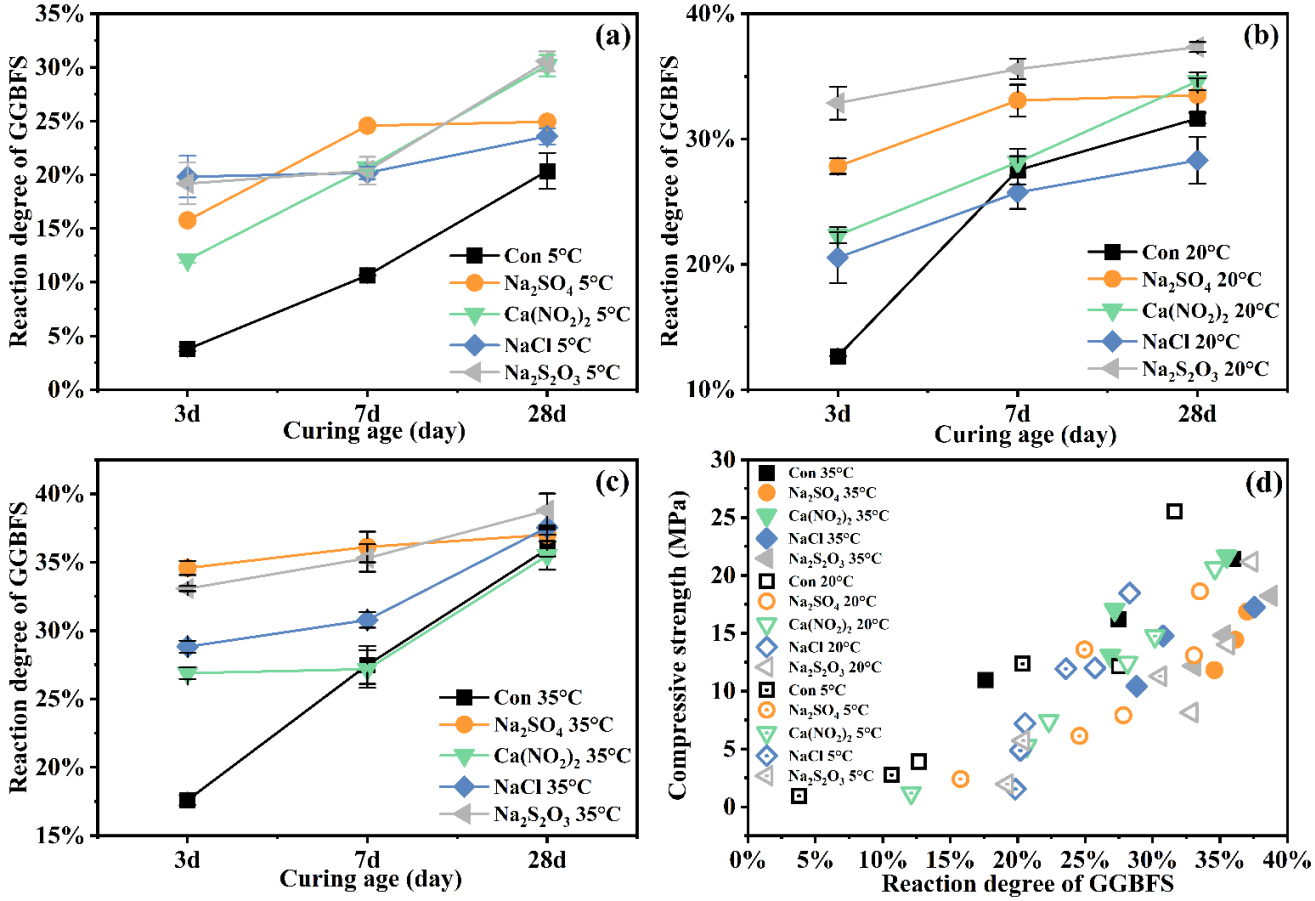

Fig. 8. Hydration degrees of pastes cured at (a) 5°C, (b) 20°C, (c) 35°C, and (d) relationship between compressive strength and hydration degree.

3.6.MIP

Fig. 9(a) shows the pore-size distribution of pastes at 3 and 28 days cured at 20 and 35°C. In a previous study, the effects of low curing temperature (5 °C) on the pore-size distribution were investigated, as shown in Fig. S4 [44]. Evident differences can be observed in the pore-size distribution curves. After 3 days of hydration, the shapes of all the curves were differentiated into two distinctly different curves wherein the right peak (at ~800 nm) indicates the critical radii at which maximal intrusion of the connected porosity first occurs [73]. The critical peak is smaller in the presence of additional activators, especially in $Na_2S_2O_3$, wherein the peak shifts to 250 nm. Compared with the curing at 20°C, the critical radii of samples cured at 35°C are smaller, which indicates that at an early age, activators and higher curing temperature promote the hydration of GGBFS and make the pores finer at an early age. However, at 28 days, the critical radii of all the samples added with activators cured at 35°C were larger than those of the samples cured at 20°C (Fig. 9(d)); the critical

radii reduced considerably, which may indicate that the higher curing temperature cannot effectively refine the pore size at a later age.

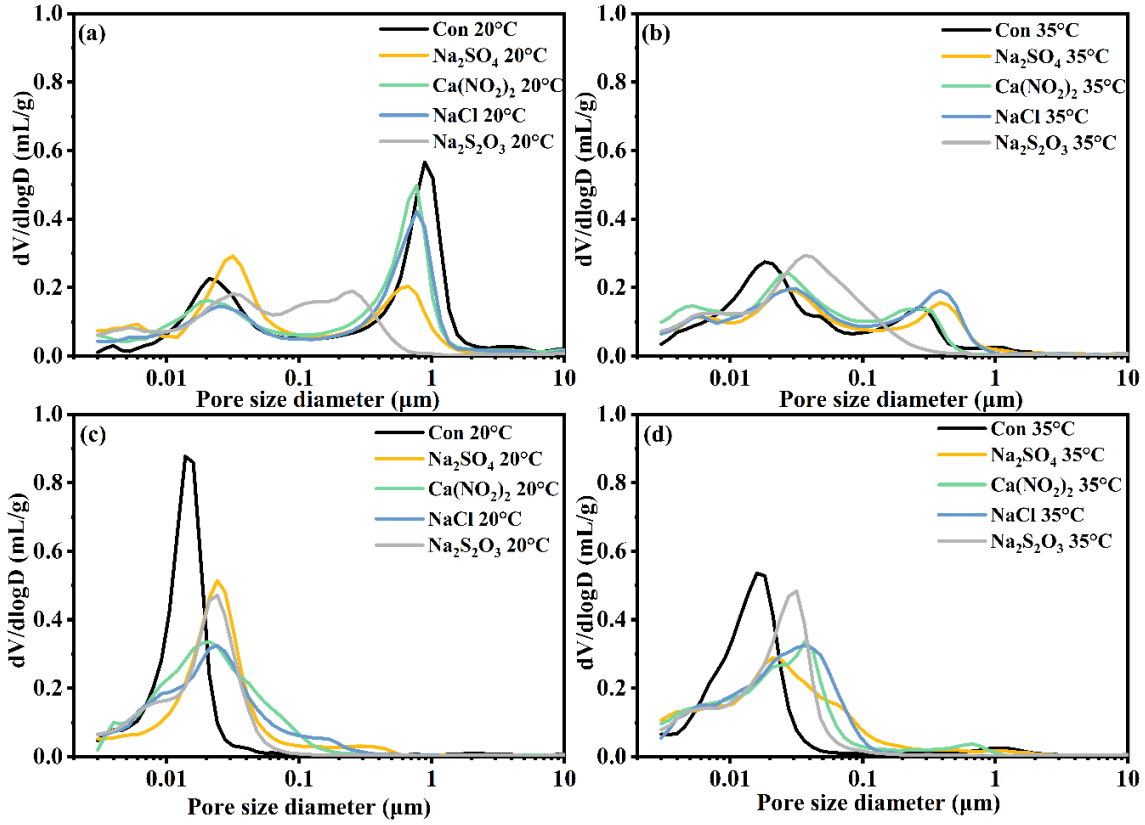

Fig. 9. MIP results of pastes. Pore size distributions of (a) pastes cured for 3 days at 20°C, (b) pastes curd for 28 days cured at 35°C, (c) pastes cured for 3 days at 35°C, and (d) pastes cured for 28 days at 35°C.

Generally, capillary pores and gel pores are defined based on the magnitude of the effect on strength development and permeability. In this study, a pore radius of 10 nm was selected to divide capillary pores and gel pores [74,75]. The total porosity and capillary porosity are shown in Fig. 10. Evidently, the total porosity decreases, and the gel pore percentage in total pore volume increases from 3 to 28 days at 5 and 20°C, thus indicating the formation of a denser matrix with a refined pore structure. At 3 days, the reaction rate of GGBFS was accelerated as a function of the curing temperature (Fig. 8). Following the formation pf reaction products, the microstructure appeared to be refined. For the samples cured at 35 °C, the total porosity was already comparable to that cured at 5 and 20 °C at 28 days. However, the volumes of the capillary pores in the samples which contained activators were larger than that of the control group at a later age, especially at higher curing temperatures. This indicates the tendency of reduction in the refining of the capillary porosity. This agrees with the result of compressive strength shown in Fig. 3.

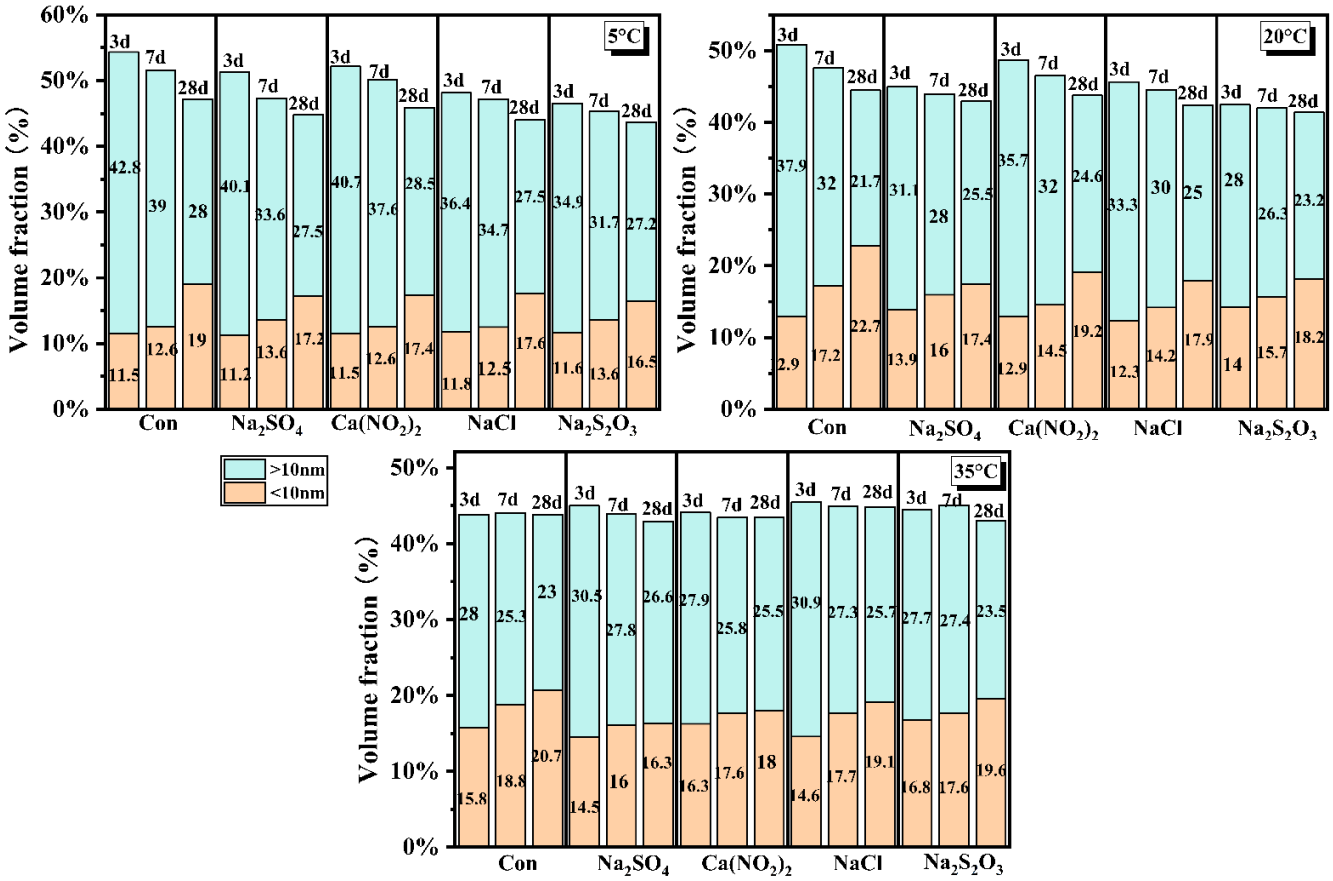

Fig. 10. Total and capillary porosities of pastes at different curing temperatures.

A comparison of the capillary porosity as a function of compressive strength is presented in Fig. 11. The plots of the capillary porosity and measured compressive strength show good agreement. Compressive strength is closely related to the capillary porosity at the early stage. An interesting phenomenon pertains to the fact that this correlation not only decreases as a function of the curing time, but also gradually worsens as a function of the curing temperature, especially at a curing temperature of 35°C; this irregular relationship began at the 3 days of curing, and may be related to the shell formation at the surface of the unreacted GGBFS caused by early hydrates. With regard to 28 days, the research of Briki et al. [76] showed that at the later stages of hydration, the reaction of GGBFS was related to the limiting pore size suitable for C-S-H growth and to the concentration of the solution in the pores. Hydrates can only grow in water-filled pores. In the cases of capillary pores, the water was consumed by hydration and contained vapor or stayed empty. Although the total porosity decreased at the late stage with the development of hydration, and the percentage of gel pore gradually increased, the small pores filled with the solution slowed down the reaction rate of the GGBFS because an increasing curvature is needed for the gel pore to grow into smaller pores;

therefore, in the later stage of hydration, the porosity cannot fully reflect the hydration degree of GGBFS and the strength of the paste. In the future, further investigations of the relative humidity will be conducted to provide acomprehensive explanation of this influence.

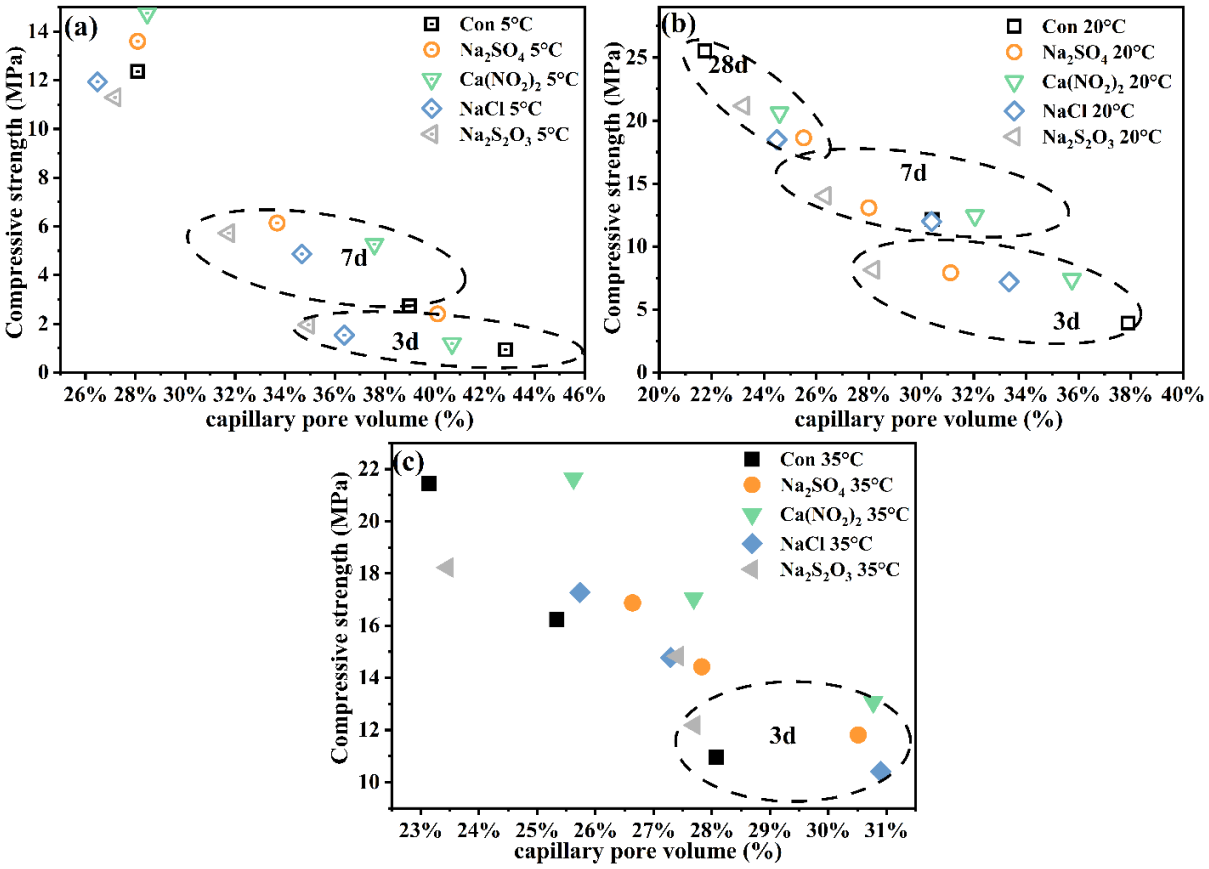

Fig. 11. Temperature plotss of compressive strength and calculated capillary porosity. Samples cured at (a)5°C, (b) 20°C, and (c) at 35°C.

4. Effects of curing temperature and activators on the initial hydration process of GGBFS

As discussed in the previous sections, although some slight differences exist in the development of reaction degree and microstructure at late ages, the influence of this difference is limited. However, the various properties of GGBFS at the early age are affected more significantly. Thus, the mechanism of the effect of the curing temperature with the use of additional activators needs to be studied further.

4.1.Thermodynamic modeling

The phase assemblage of pastes cured at 20°C (5 and 35°C in Fig. S5 and Fig. S6) was calculated based on the results of selective dissolution, and is plotted in Fig. 12. Because

478 there is no U-phase information in the database, it is difficult to simulate the phase changes
479 with this model, but the amount of U-phase is very small (Fig. 4). This has a minor impact
480 on the subsequent calculation of porosity. Compared with Con, other samples produced more
481 hydration products, especially C-S-H, which provided a lot of support for the early strength.
482 These outcomes are consistent with the XRD results shown in section 3.2. Straetlingite was
483 formed in the simulation but it was not observed in XRD. This may be because the amount
484 of Straetlingite was too small or may relate to the kinetic limitations.

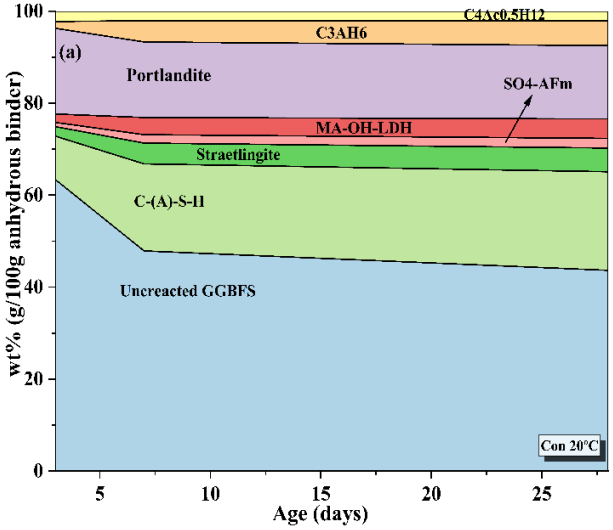

485

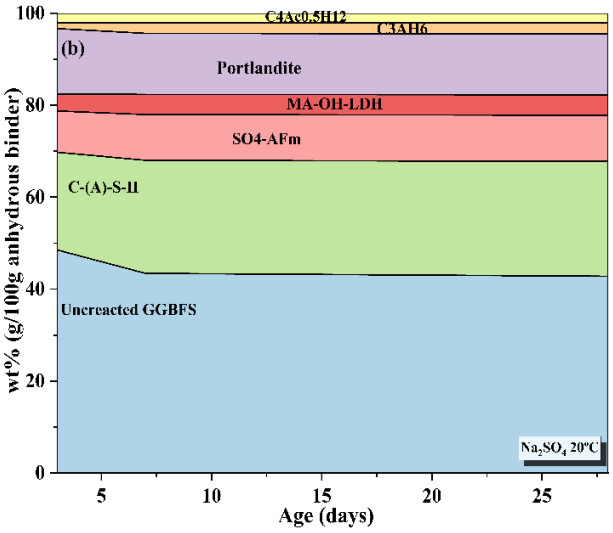

486

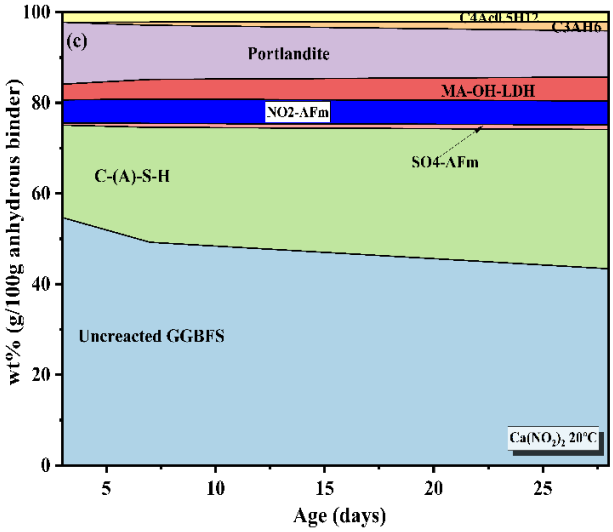
(c)
Portlandite
MA-OH-LDH
NO2-AFm
SO4-AFm
C-(A)-S-H
Uncreacted GGBFS
Ca(NO2)2 20°C
wt% (g/100g anhydrous binder)
Age (days)

487

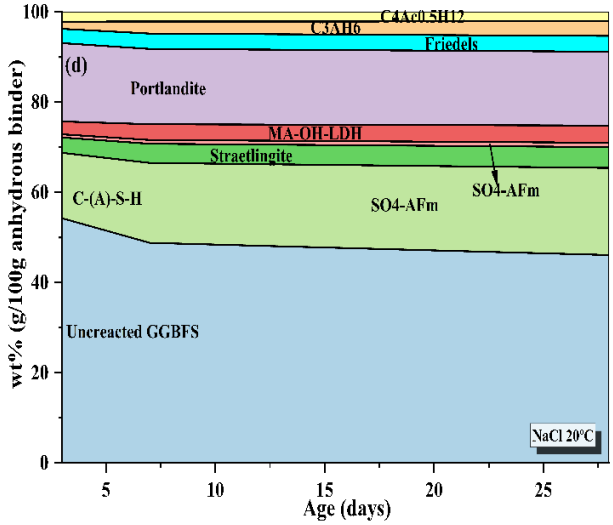
(d)
C4Ac0.5H12
C3AH6
Friedels
Portlandite
MA-OH-LDH
Straetlingite
SO4-AFm
C-(A)-S-H
SO4-AFm
Uncreacted GGBFS
NaCl 20°C
wt% (g/100g anhydrous binder)
Age (days)

488

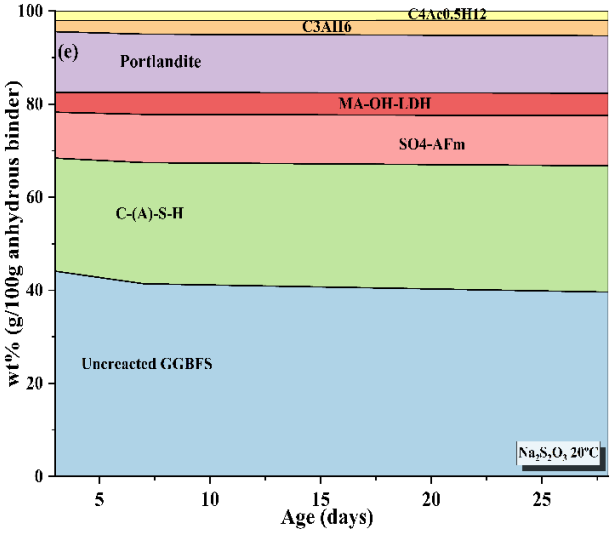

Fig. 12. Phase assemblage of pastes cured at 20°C: (a) Con, (b) Na_2SO_4, (c) $Ca(NO_2)_2$, (d) NaCl, and (e) $Na_2S_2O_3$.

The early reaction of GGBFS was easily affected by pH and Ca^{2+} activity. In this study, the amount of $Ca(OH)_2$ was very high, and there was still a large amount of portlandite precipitation even in the late hydration stage. It is necessary to consider Ca^{2+} activity because it plays an important role during the dissolution of GGBFS. Ca^{2+} activity was calculated according to the correction of concentrations,

$$\{Ca^{2+}\} = [Ca^{2+}] \cdot \gamma_{Ca^{2+}} \quad (4)$$

where $\{Ca^{2+}\}$ is the activity of Ca^{2+}, $[Ca^{2+}]$ is the concentration of Ca^{2+}, and $\gamma_{Ca^{2+}}$ is the activity coefficient of Ca^{2+}.

The activity coefficient is calculated using the extended Debye–Hueckel equation [77]:

$$\log_{\gamma_{Ca^{2+}}} = \frac{-AZ^2\sqrt{I}}{1+Ba\sqrt{I}} + bI \quad (5)$$

where z is the charge of the aqueous solution, A and B are temperature- and pressure-dependent coefficients, and I is the molar ionic strength. The calculated Ca^{2+} activity was based on the application of a logarithm for comparison purposes. The results are presented in Fig. 13. In the activities of Con and $Ca(NO_2)_2$, Ca^{2+} was higher than other samples at low-temperature curing conditions. From one viewpoint, this may be attributed to the fact that the mobility of ions was reduced at low temperature, the additional amount of Ca^{2+} in $Ca(NO_2)_2$ increased the concentration of Ca^{2+}, and the dissolution of GGBFS may have been inhibited. In a previous study [44], the hindrance of GGBFS hydration at an early age owing to the influence of low-ionic mobility and common-ion effect at low-curing temperature was observed by ^{27}Al NMR (Fig. S2). The calculated activity of Ca^{2+} was consistent with the results of a previous study. In addition, the activity of Ca^{2+} as a function of the curing temperature and age, especially for the samples with added sodium salt, because sodium ions

enhance the alkalinity of the solution. Fu et al. [23] considered the relationship between Ca^{2+} activity and pH in the GGBFS cement binder system with added Na_2SO_4. They found that in this system, the OH^- activity was controlled by the Ca^{2+} activity through the solubility limit of portlandite. Therefore, in the samples with added sodium salts, the activity of Ca^{2+} decreased owing to the increase in the early pH, and the high temperature curing further reduced the solubility of portlandite; this aggravated the decrease in Ca^{2+} activity and promoted the dissolution of GGBFS.

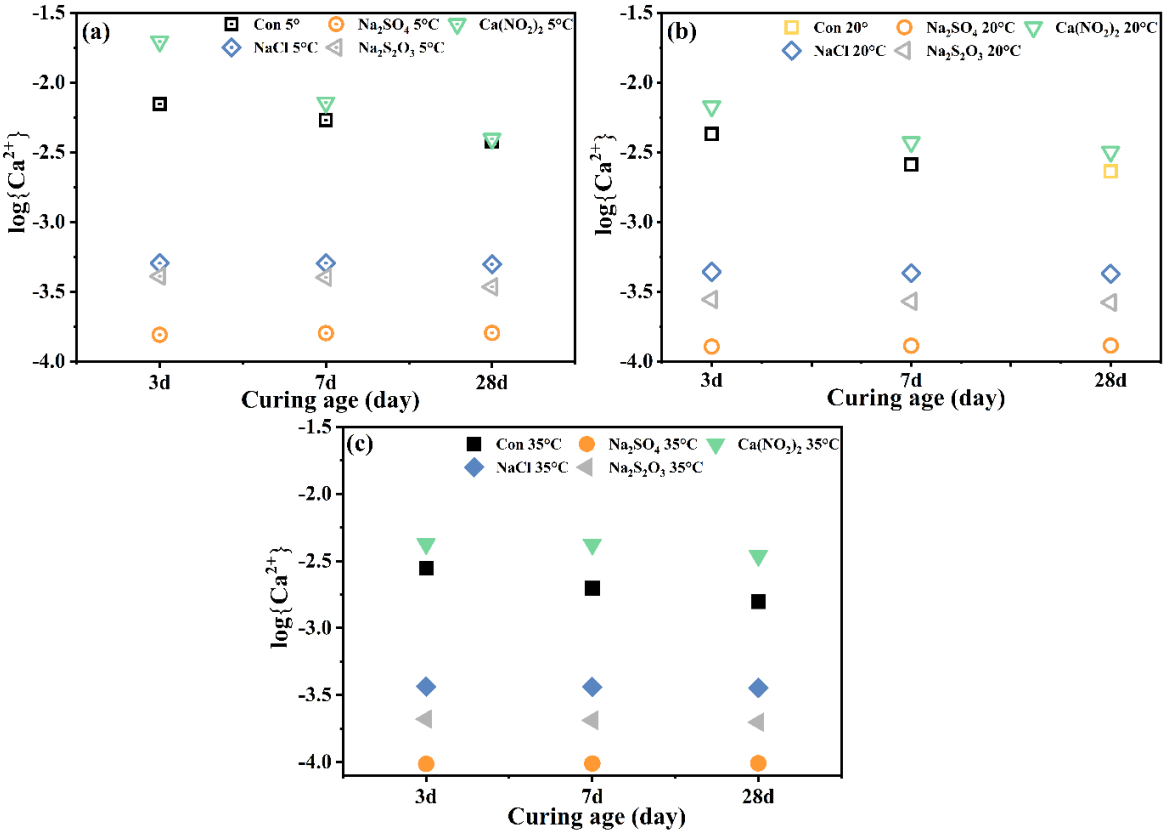

Fig. 13. Simulated activity of Ca^{2+} of pastes cured at different temperatures: Samples cured at (a) 5°C, (b) 20°C, and (c) 35°C.

4.2.Kinetics of GGBFS hydration

To characterize further the influence of the curing temperature on the GGBFS reaction. The apparent activation energy (E_a) was described by the Arrhenius equation [30, 35]:

$$\alpha = Ae^{-E_a/RT} \quad (6)$$

where α is the reaction degree of the GGBFS, A is the pre-exponential factor, R is the gas constant (8.314 J/mol/K), and T is the absolute temperature. Fig. 14 and Table 3 show the E_a values. The scale of activation energy found for the $Ca(OH)_2$-activated GGBFS system

535 ranges from 3.97 to 37.51 kJ/mol. A good linear correlation was found at an early age as
536 shown in Fig. 14, which indicates that the Arrhenius equation is suitable for studying the
537 influence of temperature and activators on GGBFS hydration at an early age. As listed in
538 Table 3, the linear correlation between the curing temperature and the degree of hydration,
539 especially at 7 days, may be related to the limited hydration degree caused by the high curing
540 temperature (Fig. 8). At 3days, there was a positive linear correlation between ln α and 1/T
541 found in all samples, indicating that the hydration degree increased with the increase in curing
542 temperature, which is consistent with the results of the hydration degree observed in Section
543 3.5. In addition, the greater the value of E_a is, the more sensitive the reaction degree of
544 GGBFS is to the change in the curing temperature. Combined with the results listed in Table
545 3, the hydrations of Con and $Ca(NO_2)_2$ samples are considerably influenced by the curing
546 temperature. This means that the high-curing temperature promotes the hydration of Con and
547 $Ca(NO_2)_2$. In the cases of the other samples, the promoting effect of high temperature is not
548 obvious owing to the promoting effect of the accelerator itself, and side effects may even
549 appear. This is consistent with the results of Ca^{2+} activity and may explain why the tendency
550 of hydration degree and compressive strength is quite different at late ages, and the decrease
551 in the rate of increase of the hydration degree. Li et al. [33] observed the "shell forming"
552 phenomenon of GGBFS hydration activated by NaOH in a high pH and temperature
553 environment based on SEM, which corresponds to the increase in E_a at increasing curing
554 temperatures, and inhibits the hydration of GGBFS enriched with the addition of sodium salts.

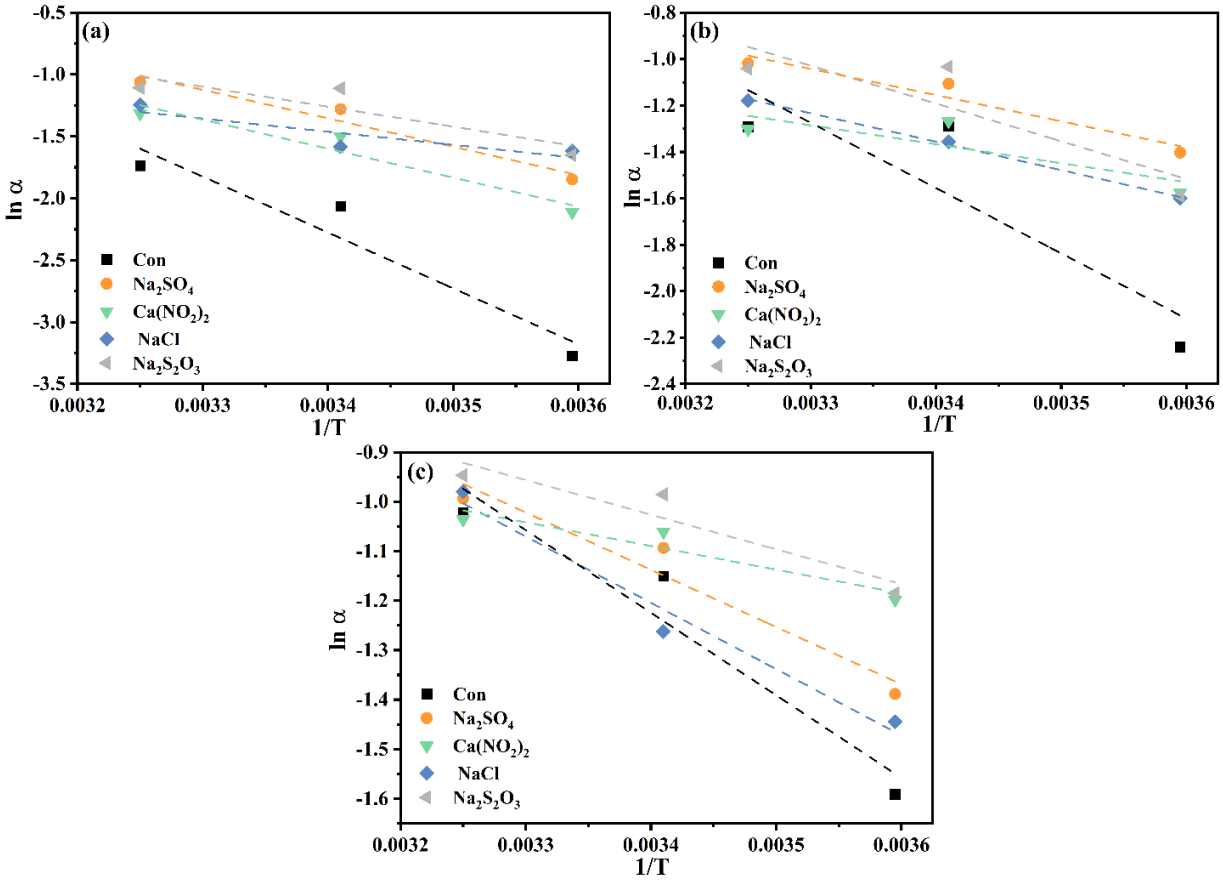

555

556 Fig. 14. Arrhenius plot of pastes cured at (a) 3 days, (b) 7 days, and (c) 28 days (note the
557 different scale of the y-axis).

558

559 Sections 3.1 and 4.1 show that the anion of the accelerator plays a decisive role in the strength
560 development of GGBFS. In a previous study, the relationship between the compressive
561 strength and the category of the anion of the accelerator was elaborated by limiting the
562 equivalent ionic conductance (LEIC), which indicates ionic mobility in a solution [44]. The
563 relationship between the LEIC and E_a is shown in Fig. 15. A good linear relationship was
564 observed at 3 days after NaCl was excluded, thus implying that at early hydration, the higher
565 the mobility of the anion in the solution is, the greater is the influence on the GGBFS
566 hydration, whereas on 7 days, the trend was exactly the opposite. This may be related to the
567 high-temperature curing, which caused the more rapid early hydrates and inhibited the
568 reaction of GGBFS; the stronger the anion mobility of the accelerator is, the more obvious
569 the inhibitory effect becomes; this finding is consistent with the results of Kondo et al. [15].
570 A weak correlation was observed at 28 days. This indicates that LEIC contributes to the initial
571 strength development according to its influence on E_a.

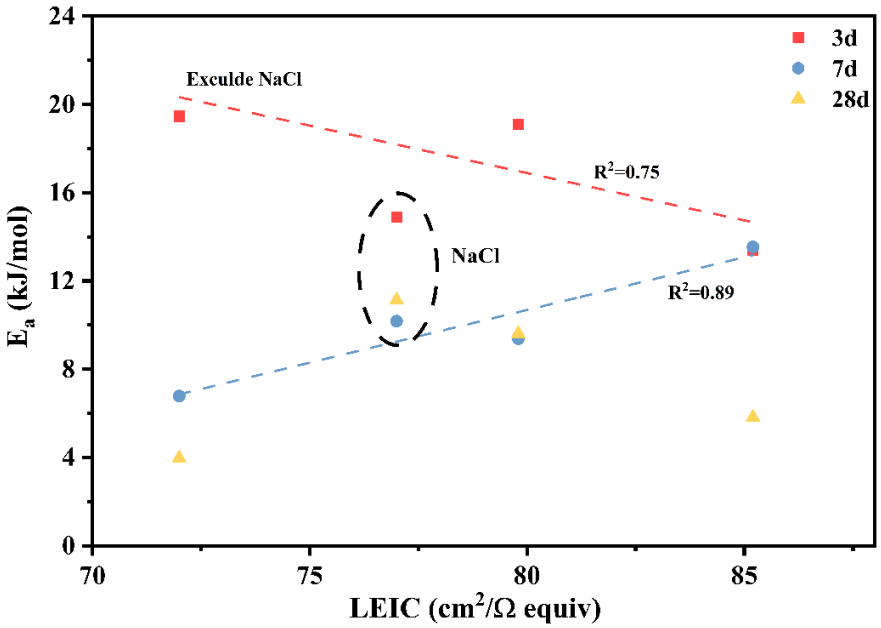

Fig. 15. Plot of the LEIC and E_a.

Table 3

Apparent activation energy of pastes enriched with the addition of different activators

Curing age	Sample	E_a (kJ/mol)	R^2
3 days	Con	37.51	0.92
	Na_2SO_4	19.10	0.96
	$Ca(NO_2)_2$	19.46	0.94
	NaCl	14.89	0.99
	$Na_2S_2O_3$	13.40	0.79
7 days	Con	23.37	0.78
	Na_2SO_4	9.38	0.93
	$Ca(NO_2)_2$	6.78	0.70
	NaCl	10.18	0.99

	$Na_2S_2O_3$	13.54	0.77
28 days	Con	13.86	0.93
	Na_2SO_4	9.61	0.95
	$Ca(NO_2)_2$	3.97	0.89
	NaCl	11.13	0.97
	$Na_2S_2O_3$	5.82	0.89

4.3.Early-stage reaction of GGBFS up to 24h

(1) Effect of activators on solid and liquid phase in $Ca(OH)_2$ activated GGBFS system

The results of the above section show that the accelerator can effectively promote the early strength of GGBFS, especially at 20°C. The $Ca(OH)_2$ activated the GGBFS system, which is quite different from the GGBFS cement system, and hydrated faster at 1 day [78]. To illustrate further the mechanism and understand what caused the promotion of GGBFS hydration, the pH value of the pore solution of samples cured at 20°C for 24 h was measured. Sodium salts increased the pH value of the pore solution at an early age (Fig. 16), while the hydration of GGBFS in cement binder or alkali-activated environment is dependent on the pH value [23, 72, 75, 78, 79]. Sodium salts effectively improved the pH value to promote the hydration of the GGBFS. In addition, the tendency of pH change is quite similar to the calorimetric curves; this indicates that pH affects the hydration of GGBFS in the $Ca(OH)_2$-activated system. However, the problem is what caused the pH increase in the pastes with added sodium salts.

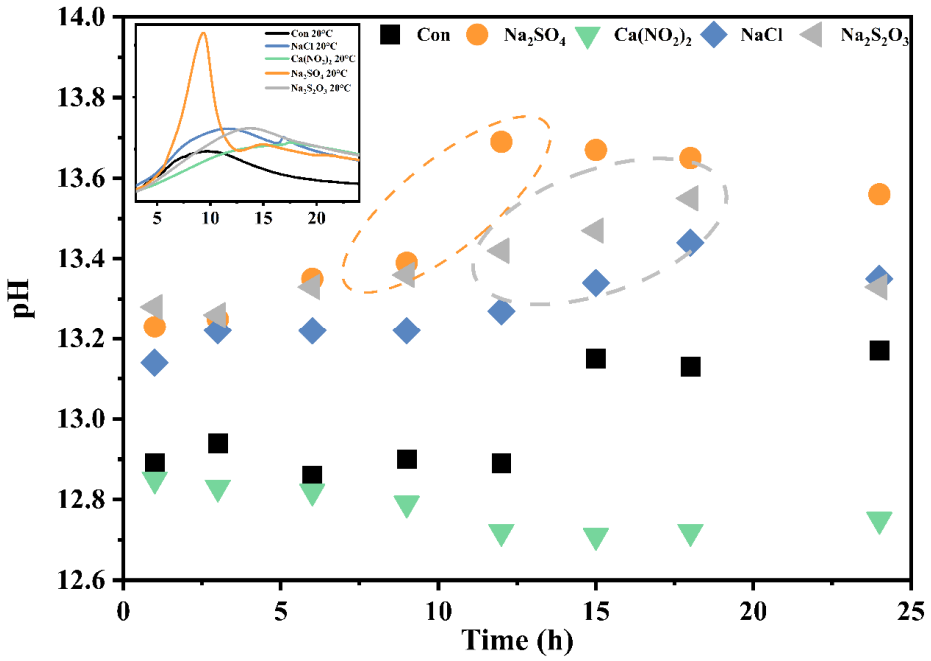

Fig. 16. Plots of pH values of pastes cured at 20°C from 1 h to 24 h.

Na_2SO_4 it mainly increases the pH value and promotes GGBFS dissolution by synergistic reaction, as shown in the following formula [80]:

$$Na_2SO_4 + Ca(OH)_2 + 2H_2O \rightarrow CaSO_4.2H_2O \downarrow + 2Na^+ + 2OH^- \quad (7)$$

In the case of NaCl, it is reported that the formation of Friedel's salt will not change the pH value because this reaction only involves the ion exchange between Cl^- and SO_4^{2-} or CO_3^{2-} [64]. NaCl increased the pH value due to the reaction between NaCl and $Ca(OH)_2$, which is in excess in this system. The formed NaOH will increase the pH value.

Regarding the $Na_2S_2O_3$, an initial high pH value in the pore solution may benefit from the fact that Na^+ can hardly react chemically, which needs OH^- to ensure charge neutrality. The high-pH value converts AFt to the U-phase and ensures the stability of the U-phase [65], which will cause a decline in the proportion of Na^+ and reduce the pH value. The lowered pH reverses the conversion above and leads to the co-existence of the U-phase and AFt as described above [65]:

$$C_4A\hat{S}_3H_{32} \rightarrow U\ phase(\rightarrow C_4AH_{13}) \rightarrow C_4A\hat{S}H_{12} \rightarrow C_4A\hat{S}_3H_{32} \quad (8)$$

This process makes the pH a little bit lower than that of Na_2SO_4 but higher than other activators. The result of ion chromatography also favors this conclusion. Ion chromatography was used to measure the Na^+ and Ca^{2+} of Con, Na_2SO_4, $Ca(NO_2)_2$, and $Na_2S_2O_3$ cured at 20°C for 18 h. Fig. 17(a) shows the Na^+ changes and compares the concentrations of Na_2SO_4 and $Na_2S_2O_3$, confirming that sufficient Na^+ remained in the pore solution, which required OH^- to ensure charge neutrality. Fig. 17(b) shows the Ca^{2+} concentration changes at 20°C during the initial 18 h. The Ca^{2+} concentration in $Ca(NO_2)_2$ is relatively higher than that of other

615 samples. Fig. 18 confirms that a certain amount of portlandite precipitation is produced
616 during early hydration, which is why the pH value of $Ca(NO_2)_2$ is quite low at the initial
617 stage, eventhough some Ca^{2+} is consumed in the form of AFm, which means that high Ca^{2+}
618 may inhibit the dissolution of $Ca(OH)_2$, inhibit the hydration of GGBFS, and may be related
619 to the high Ca^{2+} activity in the early stage.

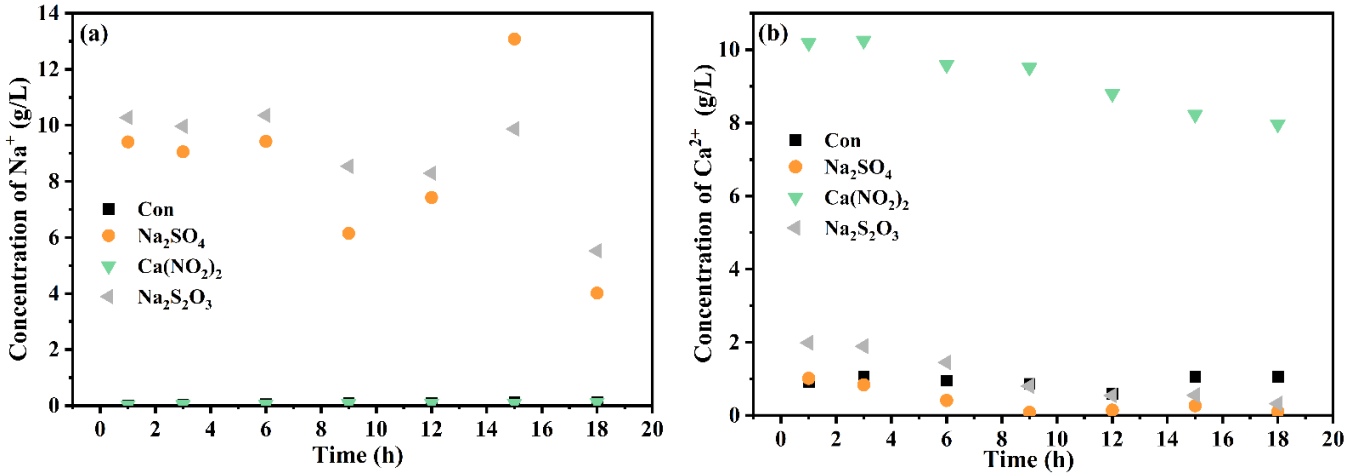

620

621 Fig. 17. Ionic concentrations of pastes as a function of time cured at 20°C: (a) Na^+ and (b)
622 Ca^{2+}.

623

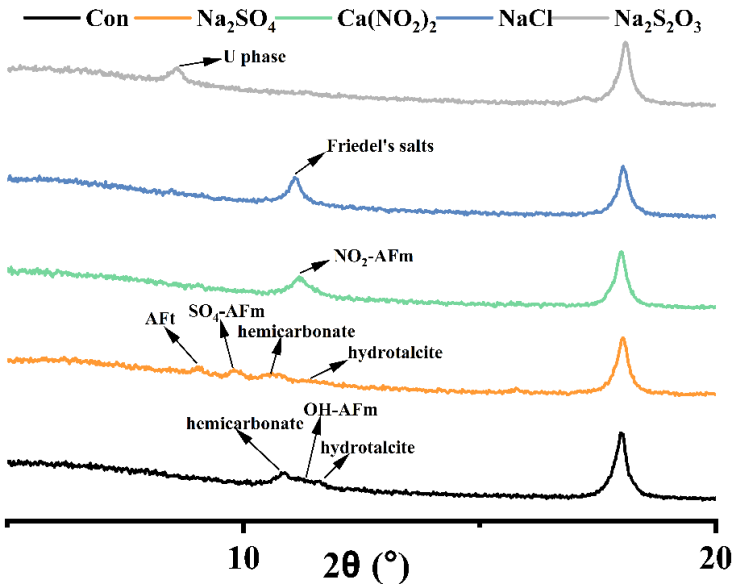

624

625 Fig. 18. XRD patterns of pastes cured for 12 h at 20°C.

626

(2) Mechanisms of the activators on the $Ca(OH)_2$-activated GGBFS at an early age

Finally, the mechanisms of the activators on the $Ca(OH)_2$-activated GGBFS at an early age are shown in Fig. 19. In contrast to other systems, both the anions and cations of activators added to the $Ca(OH)_2$-activated GGBFS system play an important role.

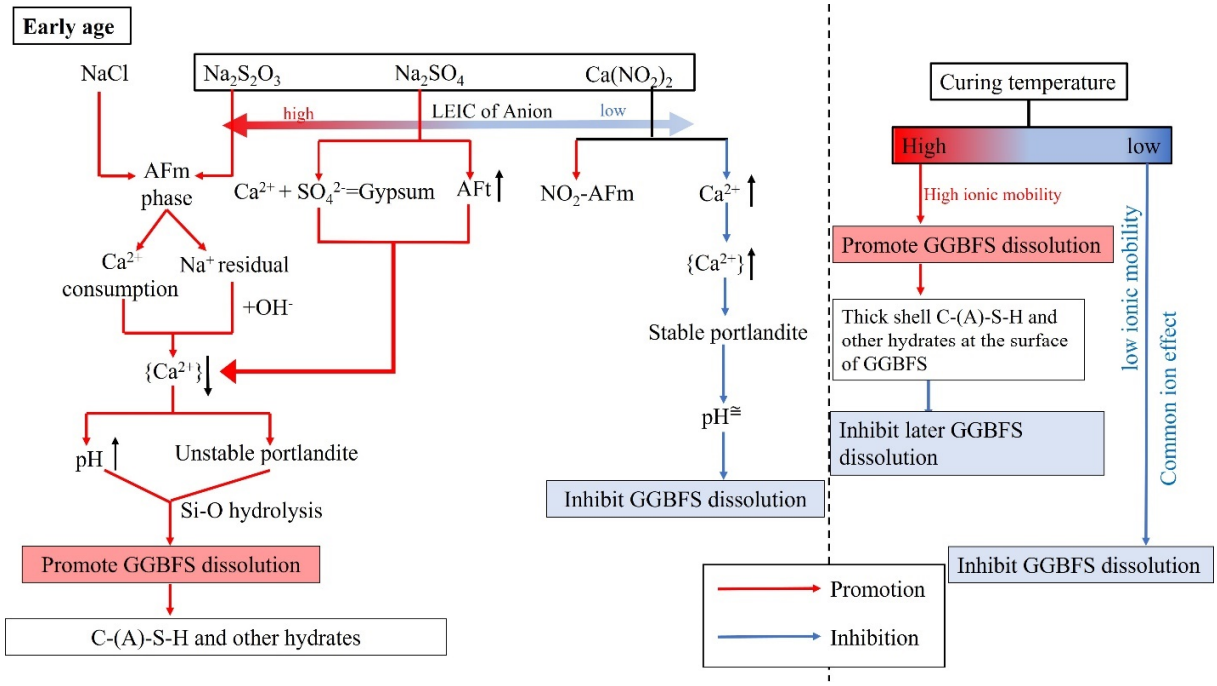

Fig. 19. Schematic coupling effects of curing temperature and activators on the hydration of GGBFS at an early age.

$NaCl$ and $Na_2S_2O_3$ increased the initial pH value because of the high-ionic mobility (as the LEIC increases, the ionic mobility decreases), and produced the AFm phase, which consumesd some Ca^{2+} to decrease the Ca^{2+} activity and produce some Na^+ residual, which needed OH^- to ensure charge neutrality.

The added Na_2SO_4, which also had high-ionic mobility, reacted with portlandite to form gypsum and NaOH; this promoted the formation of AFt and increased the pH value. The higher pH value promoted the hydrolysis of the Si-O band in GGBFS, which helped the dissolution of GGBFS and led to the formation of more C-(A)-S-H. These AFm phases and C-(A)-S-H provide strength at an early age.

In the case of $Ca(NO_2)_2$, which has a relatively low-ionic mobility, the pH value remained unchanged, or decreased slightly compared with that of Con. This is attributed to the fact that Ca^{2+} increased the activity of Ca^{2+} and inhibited the decomposition of calcium hydroxide, although NO_2–AFm was generated that inhibited the dissolution of GGBFS to some extent.

(3) Effects of curing temperature on GGBFS hydration

The most obvious effects of curing temperature is attributed to the fact that high temperature promotes the dissolution of GGBFS because they provides more energy necessary to

651 overcome the barriers to continue hydration. However, more rapid hydrates precipitate on
652 the GGBFS surface to form a thick shell, which inhibits the subsequent hydration. At the
653 low-curing temperature, $Ca(NO_2)_2$ further inhibits the hydration of GGBFS at an early age
654 owing to the influence of low-ionic mobility and the common-ion effect; the latter suppresses
655 the calcium hydroxide solubility owing to the increase in the calcium concentration, and
656 causes a decrease in pH.
657

658 ## 5. Conclusions

659 In this study, the coupling effects of the curing temperature and activators on $Ca(OH)_2$
660 activated GGBFS system were investigated by XRD, isothermal calorimetry, NMR, and
661 thermodynamic modeling. The key conclusions are as follows.
662 (1) The accelerator can effectively promote the early strength of GGBFS, especially at 20°C,
663 during which NaCl has the worst promotion effects. The early strengths of the samples
664 cured at 35°C were the largest, but the later strength were significantly lower than those
665 of the same samples cured at 20°C. At low temperature, the accelerator had the most
666 obvious effect on the medium-term strength of the samples. Owing to the low-hydration
667 degree, the activator still promoted strength until a later stage. In this study, the hydrated
668 type mainly depended on the category of activators, and the different curing temperatures
669 did not change the type of hydration products, but only the quantity of hydration products.
670 (2) There was a positive linear correlation between lnα and 1/T in each hydration stage that
671 indicated that high temperature provided more energy to overcome the barriers to
672 continue hydration.
673 (3) A good correlation was observed between LEIC and E_a at an early age. At an early age,
674 the stronger the anionic mobility of the accelerator was, the more obvious the reaction
675 promotion effect on GGBFS was, while at 7 days, the trend was opposite. These findings
676 were consistent with the tendency of strength development.
677 (4) The pH showed a strong correlation with the initial hydration of the GGBFS. Before the
678 first day, the increased pH was due to the reaction in Na_2SO_4, while NaCl increased the
679 pH owing to the reaction between NaCl and the excess amount of $Ca(OH)_2$. Although a
680 certain degree of U-phase was formed, sufficient Na^+ remained in the pore solution of
681 $Na_2S_2O_3$ that required OH^- to ensure charge neutrality, and the high pH promoted early
682 hydration. In $Ca(NO_2)_2$, the pH value was quite low at the initial stage, even though some
683 Ca^{2+} was consumed in the form of AFm. Collectively, this means that high Ca^{2+} may
684 inhibit the dissolution of CH due to the common-ion effect, thereby inhibiting the
685 hydration of GGBFS.
686 (5) The effects were different at different curing temperatures. In a previous study, we
687 confirmed at low-curing temperature, because of the influences of low-ionic mobility and
688 common-ion effect, $Ca(NO_2)_2$ inhibited the hydration of GGBFS at an early age. This
689 study provided more evidence from the results of simulated Ca^{2+} activity, whereas high
690 temperature and activators promoted considerably the hydration degree at an early age.
691 Owing to the cross-over effect, the thick shell at the surface of the GGBFS formed by
692 more rapid early hydrates inhibited the late hydration.

693

694 **Declaration of Competing Interest**

695 The authors declare that they have no known competing financial interests or personal
696 relationships that could have appeared to influence the work reported in this paper.
697

698 **Funding**

699 This work was supported by JSPS KAKENHI [grant Number 21K04349] and by the Steel
700 Foundation for Environmental Protection Technology.

701 **References**

702 [1] Statista, Production volume of cement in Japan from fiscal year 2010 to 2019.
703 https://www.statista.com/statistics/678820/japan-annual-cement-production-
704 volume/#statisticContainer. (accessed August 20, 2021).

705 [2] M. Saillio, V. Baroghel-Bouny, S. Pradelle, M. Bertin, J. Vincent, J.B. d'Espinose de
706 Lacaillerie, Effect of supplementary cementitious materials on carbonation of cement pastes,
707 Cem. Concr. Res. 142 (2021). https://doi.org/10.1016/j.cemconres.2021.106358.

708 [3] V. Kocaba, E. Gallucci, K.L. Scrivener, Methods for determination of degree of reaction
709 of slag in blended cement pastes, Cem. Concr. Res. 42 (2012) 511–525.
710 https://doi.org/10.1016/j.cemconres.2011.11.010.

711 [4] U. De Filippis, E. Prud'homme, S. Meille, Relation between activator ratio, hydration
712 products and mechanical properties of alkali-activated slag, Constr. Build. Mater. 266 (2021).
713 https://doi.org/10.1016/j.conbuildmat.2020.120940.

714 [5] S.F.A. Shah, B. Chen, S.Y. Oderji, M.A. Haque, M.R. Ahmad, Improvement of early
715 strength of fly ash-slag based one-part alkali activated mortar, Constr. Build. Mater. 246
716 (2020). https://doi.org/10.1016/j.conbuildmat.2020.118533.

717 [6] P. Suraneni, A. Hajibabaee, S. Ramanathan, Y. Wang, J. Weiss, New insights from
718 reactivity testing of supplementary cementitious materials, Cem. Concr. Compos. 103 (2019)
719 331–338. https://doi.org/10.1016/j.cemconcomp.2019.05.017.

720 [7] E. Özbay, M. Erdemir, H.İ Durmuş, Utilization and efficiency of ground granulated blast
721 furnace slag on concrete properties—A review, Constr. Build. Mater. 105 (2016) 423–434.
722 https://doi.org/10.1016/j.conbuildmat.2015.12.153.

723 [8] P. Awoyera, A. Adesina, A critical review on application of alkali activated slag as a
724 sustainable composite binder, Case Stud. Constr. Mater. 11 (2019).
725 https://doi.org/10.1016/j.cscm.2019.e00268.

726 [9] B. Vafaei, K. Farzanian, A. Ghahremaninezhad, The influence of superabsorbent polymer
727 on the properties of alkali-activated slag pastes, Constr. Build. Mater. 236 (2020).
728 https://doi.org/10.1016/j.conbuildmat.2019.117525.

729 [10] R.J. Myers, B. Lothenbach, S.A. Bernal, J.L. Provis, Thermodynamic modelling of

730 alkali-activated slag cements, Appl. Geochem. 61 (2015) 233–247.
731 https://doi.org/10.1016/j.apgeochem.2015.06.006.

732 [11] J. Wang, P. Du, Z. Zhou, D. Xu, N. Xie, X. Cheng, Effect of nano-silica on hydration,
733 microstructure of alkali-activated slag, Constr. Build. Mater. 220 (2019) 110–118.
734 https://doi.org/10.1016/j.conbuildmat.2019.05.158.

735 [12] W.S. Yum, J.Il. Suh, D. Jeon, J.E. Oh, Strength enhancement of CaO-activated slag
736 system through addition of calcium formate as a new auxiliary activator, Cem. Concr.
737 Compos. 109 (2020). https://doi.org/10.1016/j.cemconcomp.2020.103572.

738 [13] W.S. Yum, J.Il. Suh, S. Sim, S. Yoon, Y. Jun, J.E. Oh, Influence of calcium and sodium
739 nitrate on the strength and reaction products of the CaO-activated GGBFS system, Constr.
740 Build. Mater. 215 (2019) 839–848. https://doi.org/10.1016/j.conbuildmat.2019.04.240.

741 [14] Y. Jeong, J.E. Oh, Y. Jun, J. Park, J.H. Ha, S.G. Sohn, Influence of four additional
742 activators on hydrated-lime [Ca(OH)2] activated ground granulated blast-furnace slag, Cem.
743 Concr. Compos. 65 (2016) 1–10. https://doi.org/10.1016/j.cemconcomp.2015.10.007.

744 [15] R. Kondo, C.T. Song, S. Goto, M. Daimon, The Latent hydraulic property of granulated
745 blast furnace slag by various activators, Tetsu-to-Hagane. 65 (1979) 1825–1829.
746 https://doi.org/10.2355/tetsutohagane1955.65.13_1825.

747 [16] B.S. Gebregziabiher, R.J. Thomas, S. Peethamparan, Temperature and activator effect
748 on early-age reaction kinetics of alkali-activated slag binders, Constr. Build. Mater. 113
749 (2016) 783–793. https://doi.org/10.1016/j.conbuildmat.2016.03.098.

750 [17] F. Cihangir, B. Ercikdi, A. Kesimal, H. Deveci, F. Erdemir, Paste backfill of high-
751 sulphide mill tailings using alkali-activated blast furnace slag: Effect of activator nature,
752 concentration and slag properties, Miner. Eng. 83 (2015) 117–127.
753 https://doi.org/10.1016/j.mineng.2015.08.022.

754 [18] R. Kondo, M. Daimon, E. Sakai, H. Ushiyama, Influence of inorganic salts on the
755 hydration of tricalcium silicate, J. Biochem. Toxicol. 27 (1977) 191–197.
756 https://doi.org/10.1002/jbt.2570270128.

757 [19] S.J. Bae, S. Park, H.K. Lee, Role of Al in the crystal growth of alkali-activated fly ash
758 and slag under a hydrothermal condition, Constr. Build. Mater. 239 (2020).
759 https://doi.org/10.1016/j.conbuildmat.2019.117842.

760 [20] S. Park, H.M. Park, H.N. Yoon, J. Seo, C.M. Yang, J.L. Provis, B. Yang, Hydration
761 kinetics and products of MgO-activated blast furnace slag, Constr. Build. Mater. 249 (2020).
762 https://doi.org/10.1016/j.conbuildmat.2020.118700.

763 [21] Y. Zuo, M. Nedeljković, G. Ye, Coupled thermodynamic modelling and experimental
764 study of sodium hydroxide activated slag, Constr. Build. Mater. 188 (2018) 262–279.
765 https://doi.org/10.1016/j.conbuildmat.2018.08.087.

766 [22] B. Lothenbach, D.A. Kulik, T. Matschei, M. Balonis, L. Baquerizo, B. Dilnesa, G.D.
767 Miron, R.J. Myers, Cemdata18: A chemical thermodynamic database for hydrated Portland

768 cements and alkali-activated materials, Cem. Concr. Res. 115 (2019) 472–506.
769 https://doi.org/10.1016/j.cemconres.2018.04.018.

770 [23] J. Fu, A.M. Jones, M.W. Bligh, C. Holt, L.M. Keyte, F. Moghaddam, S.J. Foster, T.D.
771 Waite, Mechanisms of enhancement in early hydration by sodium sulfate in a slag-cement
772 blend—Insights from pore solution chemistry, Cem. Concr. Res. 135 (2020).
773 https://doi.org/10.1016/j.cemconres.2020.106110,
774 http://www.ncbi.nlm.nih.gov/pubmed/106110.

775 [24] K.H. Yang, K.H. Lee, J.K. Song, M.H. Gong, Properties and sustainability of alkali-
776 activated slag foamed concrete, J. Clean. Prod. 68 (2014) 226–233.
777 https://doi.org/10.1016/j.jclepro.2013.12.068.

778 [25] Z. Chen, H. Ye, Sequestration and release of nitrite and nitrate in alkali-activated slag:
779 A route toward smart corrosion control, Cem. Concr. Res. 143 (2021).
780 https://doi.org/10.1016/j.cemconres.2021.106398,
781 http://www.ncbi.nlm.nih.gov/pubmed/106398.

782 [26] H. Yu, Y. Yi, C. Unluer, Heat of hydration, bleeding, viscosity, setting of Ca(OH)2-
783 GGBS and MgO-GGBS grouts, Constr. Build. Mater. 270 (2021).
784 https://doi.org/10.1016/j.conbuildmat.2020.121839.

785 [27] W.S. Yum, Y. Jeong, H. Song, J.E. Oh, Recycling of limestone fines using Ca(OH)2-
786 and Ba(OH)2-activated slag systems for eco-friendly concrete brick production, Constr.
787 Build. Mater. 185 (2018) 275–284. https://doi.org/10.1016/j.conbuildmat.2018.07.112.

788 [28] S.A. Bernal, R.S. Nicolas, J.S.J. Van Deventer, J.L. Provis, Alkali-activated slag
789 cements produced with a blended sodium carbonate/sodium silicate activator, Adv. Cem. Res.
790 28 (2016) 262–273. https://doi.org/10.1680/jadcr.15.00013.

791 [29] K.H. Yang, J.Il. Sim, S.H. Nam, Enhancement of reactivity of calcium hydroxide-
792 activated slag mortars by the addition of barium hydroxide, Constr. Build. Mater. 24 (2010)
793 241–251. https://doi.org/10.1016/j.conbuildmat.2009.09.001.

794 [30] J.J. Biernacki, J.M. Richardson, P.E. Stutzman, D.P. Bentz, Kinetics of slag hydration
795 in the presence of calcium hydroxide, J. Am. Ceram. Soc. 85 (2002) 2261–2267.
796 https://doi.org/10.1111/j.1151-2916.2002.tb00445.x.

797 [31] M. Ben Haha, G. Le Saout, F. Winnefeld, B. Lothenbach, Influence of activator type on
798 hydration kinetics, hydrate assemblage and microstructural development of alkali activated
799 blast-furnace slags, Cem. Concr. Res. 41 (2011) 301–310.
800 https://doi.org/10.1016/j.cemconres.2010.11.016.

801 [32] G. Sun, J. Zhang, N. Yan, Microstructural evolution and characterization of ground
802 granulated blast furnace slag in variant pH, Constr. Build. Mater. 251 (2020).
803 https://doi.org/10.1016/j.conbuildmat.2020.118978.

804 [33] P. Li, J. Tang, Y. Bai, X. Chen, J. Chen, Experimental study on the pH for activating
805 ground granulated blast-furnace slag activity at different temperatures, Sādhanā. 44 (2019).
806 https://doi.org/10.1007/s12046-019-1204-z.

807 [34] D. Shi, Y. Yao, J. Ye, W. Zhang, Effects of seawater on mechanical properties,
808 mineralogy and microstructure of calcium silicate slag-based alkali-activated materials,
809 Constr. Build. Mater. 212 (2019) 569–577.
810 https://doi.org/10.1016/j.conbuildmat.2019.03.288.

811 [35] P. Li, J. Tang, X. Chen, Y. Bai, Q. Li, Effect of temperature and pH on early hydration
812 rate and apparent activation energy of alkali-activated slag, Adv. Mater. Sci. Eng. 2019 (2019)
813 1–13. https://doi.org/10.1155/2019/3531543.

814 [36] T. Medina-Serna, S. Arredondo-Rea, J. Gómez-Soberón, C. Rosas-Casarez, R. Corral-
815 Higuera, Effect of curing temperature in the alkali-activated blast-furnace slag paste and their
816 structural influence of porosity, Adv. Sci. Technol. Res. J. 10 (2016) 74–79.
817 https://doi.org/10.12913/22998624/64021.

818 [37] K. Federowicz, V.A. Figueiredo, H. Al-Kroom, H.A. Abdel-Gawwad, M.A. Abd
819 Elrahman, P. Sikora, The effects of temperature curing on the strength development,
820 transport properties, and freeze–thaw resistance of blast furnace slag cement mortars
821 modified with nanosilica, Materials (Basel). 13 (2020). https://doi.org/10.3390/ma13245800.

822 [38] E.D. Shumuye, J. Zhao, Z. Wang, Effect of the curing condition and high-temperature
823 exposure on ground-granulated blast-furnace slag cement concrete, Int. J. Concr. Struct.
824 Mater. 15 (2021). https://doi.org/10.1186/s40069-020-00437-6.

825 [39] D.P. Bentz, P.E. Stutzman, F. Zunino, Low-temperature curing strength enhancement in
826 cement-based materials containing limestone powder, Mater. Struct. 50 (2017).
827 https://doi.org/10.1617/s11527-017-1042-6.

828 [40] K. Yang, Y. Yang, X. Li, Z. Zhao, F. Wu, Hydration behaviour and early microstructure
829 of alkali-activated slag binder at low temperature, Jianzhu Cailiao Xuebao J. Build. Mater.
830 23 (2020). https://doi.org/10.3969/j.issn.1007-9629.2020.05.001.

831 [41] Z. Liu, B. Lou, D.M. Barbieri, A. Sha, T. Ye, Y. Li, Effects of pre-curing treatment and
832 chemical activators on Portland cement mortars at low temperature (5 °C), Constr. Build.
833 Mater. 240 (2020). https://doi.org/10.1016/j.conbuildmat.2019.117893.

834 [42] X. Wei, D. Li, F. Ming, C. Yang, L. Chen, Y. Liu, Influence of low-temperature curing
835 on the mechanical strength, hydration process, and microstructure of alkali-activated fly ash
836 and ground granulated blast furnace slag mortar, Constr. Build. Mater. 269 (2021).
837 https://doi.org/10.1016/j.conbuildmat.2020.121811.

838 [43] I.H. Aziz, M.M.Al. Bakri Abdullah, M.A.A.Mohd. Salleh, S. Yoriya, J. Chaiprapa, C.
839 Rojviriya, L.Y. Li, Microstructure and porosity evolution of alkali activated slag at various
840 heating temperatures, J. Mater. Res. Technol. 9 (2020).
841 https://doi.org/10.1016/j.jmrt.2020.11.041.

842 [44] Q. Zhai, K. Kurumisawa, Effect of accelerators on Ca(OH)2 activated ground granulated
843 blast-furnace slag at low curing temperature, Cem. Concr. Compos. 124 (2021).
844 https://doi.org/10.1016/j.cemconcomp.2021.104272.

845 [45] M. Ojima, K. Sasaki, K. Kurumisawa, EFFECT OF accelerating admixture ON EARLY

846 STRENGTH DEVELOPMENT OF BLAST-FURNACE SLAG CEMENT PASTE, Cement
847 Science and Concrete Technology. 72 (2019) 114–121.
848 https://doi.org/10.14250/cement.72.114.

849 [46] R. Du, X. Zhang, M. Gu, T. Ji, The Composition Effect and Mechanism of
850 Polycarboxylate Superplasticizers and Early Strength Agent, Cailiao Daobao/Materials
851 Reports. 33. https://doi.org/10.11896/cldb.18040139, 2019.

852 [47] X. Yu, C. Yu, Q. Jiang, Q. Ran, J. Liu, B. Yang, In-Situ X-Ray Diffraction Analysis on
853 the Role of Hardening Accelerator in Early Hydration of Cement, Cailiao Daobao/Materials
854 Reports. 34. https://doi.org/10.11896/cldb.19010051, 2020.

855 [48] Y. Yamada, K. Kurumisawa, IMPROVEMENT OF INITIAL STRENGTH OF BLAST
856 FURNACE SLAG CEMENT PASTE USING FROST DAMAGE INHIBITOR BY
857 ACCELERATOR, Cement Science and Concrete Technology. 73 (2020) 103–110.
858 https://doi.org/10.14250/cement.73.103.

859 [49] X. Dai, S. Aydın, M.Y. Yardımcı, K. Lesage, G. De Schutter, Effect of ca(Oh)2 addition
860 on the engineering properties of sodium sulfate activated slag, Materials (Basel). 14 (2021).
861 https://doi.org/10.3390/ma14154266.

862 [50] S. Joseph, J. Skibsted, Ö. Cizer, Hydration of polyphase Ca3SiO5-Ca3Al2O6 in the
863 presence of gypsum and Na2SO4, J. Am. Ceram. Soc. 103 (2020) 6461–6474.
864 https://doi.org/10.1111/jace.17321.

865 [51] S.A. Bernal, M.C.G. Juenger, X. Ke, W. Matthes, B. Lothenbach, N. De Belie, J.L.
866 Provis, Characterization of supplementary cementitious materials by thermal analysis, Mater.
867 Struct. 50 (2017). https://doi.org/10.1617/s11527-016-0909-2.

868 [52] Y.A. Villagrán-Zaccardi, A. Vollpracht, E. Gruyaert, N. De Belie, Recommendation of
869 RILEM TC 238-SCM: Determination of the degree of reaction of siliceous fly ash and slag
870 in hydrated cement paste by the selective dissolution method, Mater. Struct. 51 (2018).
871 https://doi.org/10.1617/s11527-017-1134-3.

872 [53] Z. Bian, G. Jin, T. Ji, Effect of combined activator of Ca(OH)2 and Na2CO3 on
873 workability and compressive strength of alkali-activated ferronickel slag system, Cem. Concr.
874 Compos. 123 (2021). https://doi.org/10.1016/j.cemconcomp.2021.104179,
875 http://www.ncbi.nlm.nih.gov/pubmed/104179.

876 [54] J.S. Lumley, R.S. Gollop, G.K. Moir, H.F.W. Taylor, Degrees of reaction of the slag in
877 some blends with Portland cements, Cem. Concr. Res. 26 (1996) 139–151.
878 https://doi.org/10.1016/0008-8846(95)00190-5.

879 [55] A. Bougara, C. Lynsdale, N.B. Milestone, The influence of slag properties, mix
880 parameters and curing temperature on hydration and strength development of slag/cement
881 blends, Constr. Build. Mater. 187 (2018) 339–347.
882 https://doi.org/10.1016/j.conbuildmat.2018.07.166.

883 [56] T.T. Tran, H. Kang, H.M. Kwon, Effect of heat curing method on the mechanical
884 strength of alkali-activated slag mortar after high-temperature exposure, Materials (Basel).

12 (2019). https://doi.org/10.3390/ma12111789.

[57] C. Korde, M. Cruickshank, R.P. West, C. Pellegrino, Activated slag as partial replacement of cement mortars: Effect of temperature and a novel admixture, Constr. Build. Mater. 216 (2019) 506–524. https://doi.org/10.1016/j.conbuildmat.2019.04.172.

[58] K. Ezziane, A. Bougara, A. Kadri, H. Khelafi, E. Kadri, Compressive strength of mortar containing natural pozzolan under various curing temperature, Cem. Concr. Compos. 29 (2007) 587–593. https://doi.org/10.1016/j.cemconcomp.2007.03.002.

[59] R. Snellings, A. Machner, G. Bolte, H. Kamyab, P. Durdzinski, P. Teck, M. Zajac, A. Muller, K. de Weerdt, M.B. Haha, Hydration kinetics of ternary slag-limestone cements: Impact of water-to-binder ratio and curing temperature, Cem. Concr. Res. 151 (2022). https://doi.org/10.1016/j.cemconres.2021.106647.

[60] L. Nedyalkova, B. Lothenbach, G. Geng, U. Mäder, J. Tits, Uptake of iodide by calcium aluminate phases (AFm phases), Appl. Geochem. 116 (2020). https://doi.org/10.1016/j.apgeochem.2020.104559.

[61] X. Xing, J. Liu, Y. Dai, M. Yang, Y. Li, Effect of chloride ion on free nitrite ion in cement, Int. J. Corros. 2018 (2018) 1–6. https://doi.org/10.1155/2018/2940953.

[62] M. Balonis, M. Mędala, F.P. Glasser, Influence of calcium nitrate and nitrite on the constitution of AFm and AFt cement hydrates, Adv. Cem. Res. 23 (2011) 129–143. https://doi.org/10.1680/adcr.10.00002.

[63] D. Li, X. Guo, Q. Tian, Z. Xu, R. Xu, L. Zhang, Synthesis and application of Friedel's salt in arsenic removal from caustic solution, Chem. Eng. J. 323 (2017) 304–311. https://doi.org/10.1016/j.cej.2017.04.073.

[64] K. De Weerdt, A. Colombo, L. Coppola, H. Justnes, M.R. Geiker, Impact of the associated cation on chloride binding of Portland cement paste, Cem. Concr. Res. 68 (2015) 196–202. https://doi.org/10.1016/j.cemconres.2014.01.027.

[65] M.J. Sánchez-Herrero, A. Fernández-Jiménez, A. Palomo, Alkaline hydration of tricalcium aluminate, J. Am. Ceram. Soc. 95 (2012) 3317–3324. https://doi.org/10.1111/j.1551-2916.2012.05348.x.

[66] A. Fernández-Jiménez, I. Garcia-Lodeiro, O. Maltseva, A. Palomo, Hydration mechanisms of hybrid cements as a function of the way of addition of chemicals, J. Am. Ceram. Soc. 102 (2019) 427–436. https://doi.org/10.1111/jace.15939.

[67] P. Padilla-Encinas, A. Palomo, M.T. Blanco-Varela, L. Fernández-Carrasco, A. Fernández-Jiménez, Monitoring early hydration of calcium sulfoaluminate clinker, Constr. Build. Mater. 295 (2021). https://doi.org/10.1016/j.conbuildmat.2021.123578.

[68] G. Li, P. Le Bescop, M. Moranville, The U phase formation in cement-based systems containing high amounts of Na2SO4, Cem. Concr. Res. 26 (1996) 27–33. https://doi.org/10.1016/0008-8846(95)00189-1.

[69] S. Nie, R.M. Thomsen, J. Skibsted, Impact of Mg substitution on the structure and

923 pozzolanic reactivity of calcium aluminosilicate (CaO-Al2O3-SiO2) glasses, Cem. Concr.
924 Res. 138 (2020). https://doi.org/10.1016/j.cemconres.2020.106231.

925 [70] G. Deng, Y. He, L. Lu, F. Wang, S. Hu, Comparison between fly ash and slag slurry in
926 various alkaline environments: Dissolution, migration, and coordination state of aluminum,
927 ACS Sustainable Chem. Eng. 9 (2021) 12109–12119.
928 https://doi.org/10.1021/acssuschemeng.1c03434.

929 [71] K.C. Reddy, K.V.L. Subramaniam, Blast furnace slag hydration in an alkaline medium:
930 Influence of sodium content and sodium hydroxide molarity, J. Mater. Civ. Eng. 32 (2020)
931 04020371. https://doi.org/10.1061/(ASCE)MT.1943-5533.0003455.

932 [72] X. Gao, Q.L. Yu, H.J.H. Brouwers, Apply 29Si, 27Al MAS NMR and selective
933 dissolution in identifying the reaction degree of alkali activated slag-fly ash composites,
934 Ceram. Int. 43 (2017) 12408–12419. https://doi.org/10.1016/j.ceramint.2017.06.108.

935 [73] J. Fu, M.W. Bligh, I. Shikhov, A.M. Jones, C. Holt, L.M. Keyte, F. Moghaddam, C.H.
936 Arns, S.J. Foster, T.D. Waite, A microstructural investigation of a Na2SO4 activated cement-
937 slag blend, Cem. Concr. Res. 150 (2021). https://doi.org/10.1016/j.cemconres.2021.106609.

938 [74] H.M. Jennings, A. Kumar, G. Sant, Quantitative discrimination of the nano-pore-
939 structure of cement paste during drying: New insights from water sorption isotherms, Cem.
940 Concr. Res. 76 (2015) 27–36. https://doi.org/10.1016/j.cemconres.2015.05.006.

941 [75] X. Chen, T. Zhang, W. Bi, C. Cheeseman, Effect of tartaric acid and phosphoric acid on
942 the water resistance of magnesium oxychloride (MOC) cement, Constr. Build. Mater. 213
943 (2019) 528–536. https://doi.org/10.1016/j.conbuildmat.2019.04.086.

944 [76] Y. Briki, M. Zajac, M.B. Ben Haha, K. Scrivener, Factors affecting the reactivity of slag
945 at early and late ages, Cem. Concr. Res. 150 (2021).
946 https://doi.org/10.1016/j.cemconres.2021.106604,
947 http://www.ncbi.nlm.nih.gov/pubmed/106604.

948 [77] J.L. Liu, C.L. Li, A generalized Debye-Hückel theory of electrolyte solutions, AIP Adv.
949 9 (2019). https://doi.org/10.1063/1.5081863.

950 [78] Z. Liu, D.w. Zhang, L. Li, J.x. Wang, N.n. Shao, D.m. Wang, Microstructure and phase
951 evolution of alkali-activated steel slag during early age, Constr. Build. Mater. 204 (2019)
952 158–165. https://doi.org/10.1016/j.conbuildmat.2019.01.213.

953 [79] C. Yang, X. Zhu, Y. Zheng, X. Yao, K. Yang, Effect of calcium hydroxide on hydration
954 process of alkali-activated slag concrete, Jianzhu Cailiao Xuebao J. Build. Mater. 20 (2017)
955 161–167. https://doi.org/10.3969/j.issn.1007-9629.2017.02.001.

956 [80] H. Justnes, T.A. Østnor, Designing alternative binders utilizing synergistic reactions, in:
957 Am. Concr. Inst. ACI Spec. Publ. (2015).

958